HAL
open science

Multi-centennial variability driven by salinity exchanges between the Atlantic and the Arctic Ocean in a coupled climate model

Weimin Jiang, Guillaume Gastineau, Francis Codron

To cite this version:

Weimin Jiang, Guillaume Gastineau, Francis Codron. Multi-centennial variability driven by salinity exchanges between the Atlantic and the Arctic Ocean in a coupled climate model. Journal of Advances in Modeling Earth Systems, 2021, 13 (3), pp.e2020MS002366. 10.1029/2020MS002366 . hal-03149635

HAL Id: hal-03149635

https://hal.sorbonne-universite.fr/hal-03149635

Submitted on 23 Feb 2021

HAL is a multi-disciplinary open access archive for the deposit and dissemination of scientific research documents, whether they are published or not. The documents may come from teaching and research institutions in France or abroad, or from public or private research centers.

L'archive ouverte pluridisciplinaire **HAL**, est destinée au dépôt et à la diffusion de documents scientifiques de niveau recherche, publiés ou non, émanant des établissements d'enseignement et de recherche français ou étrangers, des laboratoires publics ou privés.

Check for updates

Accepted Article

Multi-centennial variability driven by salinity exchanges between the Atlantic and the Arctic Ocean in a coupled climate model

Weimin Jiang[1], Guillaume Gastineau[1], Francis. Codron[1]

[1] UMR LOCEAN, Sorbonne Université/CNRS/IRD/MNHN, Paris, France

Corresponding author: W. Jiang (weimin.jiang@locean.ipsl.fr)

Key Points

- A centennial to multi-centennial variability emerges from the North Atlantic and Arctic Ocean in the IPSL-CM6A-LR model
- AMOC oscillations are driven by freshwater build-up and release in the Arctic
- The interplay between sea-ice and oceanic freshwater export modulates the salinity anomalies in the Arctic

This article has been accepted for publication and undergone full peer review but has not been through the copyediting, typesetting, pagination and proofreading process, which may lead to differences between this version and the Version of Record. Please cite this article as doi: 10.1029/2020MS002366.

This article is protected by copyright. All rights reserved.

Accepted Article

Abstract

The IPSL-CM6-LR atmosphere-ocean coupled model exhibits a pronounced multi-centennial variability of the Atlantic meridional overturning circulation (AMOC), driven by delayed freshwater accumulation and release in the Arctic. The AMOC fluctuations are preceded by salinity-driven density anomalies in the main deep convection sites in the Labrador and Greenland seas. During a strong AMOC, a combination of reduced sea-ice volume and anomalous currents reduces the freshwater export from the Arctic and leads instead to a slow accumulation of freshwater in the central Arctic. Simultaneously, the saltier Atlantic inflow through the Barents Sea results in a positive salinity anomaly in the Eastern Arctic subsurface. When the surface Central Arctic freshwater pool finally reaches the Lincoln Sea, the oceanic currents around Greenland reorganize, leading to the export of the anomalous Arctic freshwater to the North Atlantic, enhancing the stratification in deep convection sites. The AMOC then decreases, positive salinity anomalies appear in the Central Arctic, and the variability switches to the opposite phase. These AMOC and sea ice fluctuations have broader climate impacts, with a strong AMOC leading to a mean warming of about 0.4°C north of 20°N, reaching up to 1°C in the Arctic lower troposphere during winter. In all seasons, a northward displacement of the intertropical convergence zone is also simulated.

Plain Language Summary

The North Atlantic Ocean is known to have large climate fluctuations emerging from the different components of the climate system and their interactions. These fluctuations play a crucial role in the North American and European climate or the Arctic sea ice. A proper understanding of such internal variations is key to attribute the observed climate changes to anthropogenic activities or to assess the skill of decadal forecast systems. However, investigations of the long-term basin-scale variations are restrained by the limited instrumental observations. Therefore, an atmosphere-ocean general circulation model is used here to explore the low-frequency variability. This model simulates a large variability in the North Atlantic with a period between one century and one millennium. We found that this variability owes its existence to the freshwater exchanges between the North Atlantic and Arctic. Such North Atlantic variability has important impacts, as typical positive anomalies of the Atlantic oceanic northward heat transport reduce the sea-ice, warm up the whole Northern Hemisphere by 0.4°C, and shift northward the intertropical convergence zone.

1 Introduction

The North Atlantic exhibits a pronounced variability on different timescales, ranging from interannual to multi-centennial. A proper understanding of the low-frequency intrinsic variability is essential for detecting the anthropogenic climate change and assessing decadal climate forecast skills (Cassou et al., 2018). Besides, since the scarcity of instrumental measurements hampers research on variations on a multidecadal or longer timescale (Vellinga and Wu, 2004), this knowledge is also important for designing observational networks.

The Atlantic Meridional Overturning Circulation (AMOC) consists of a warm northward near-surface current and a colder southward return flow, extending over the full latitude range. It has a significant influence on climate over the North Atlantic and peripheral land masses due to the associated basin-scale meridional heat transport: a strengthening of the AMOC increases the oceanic northward heat transport and leads to a warming in the North Atlantic, extending into the Arctic (Mahajan et al., 2011; Jackson et al., 2015). The low-frequency fluctuations of the AMOC also have impacts in the Tropics and the Southern Hemisphere: a stronger AMOC and cross-equatorial northward heat transport often lead to a northward shift of the Inter-tropical convergence

This article is protected by copyright. All rights reserved.

zone (ITCZ; Vellinga and Wu, 2004; Frierson et al., 2013) and a cooling of the Southern Hemisphere (Stocker, 1998; Muir and Fedorov, 2015). The AMOC has also been linked in climate models to the multidecadal variability of the basin-wide North Atlantic sea surface temperature (SST; Roberts et al., 2013; Knight et al., 2005), known as the Atlantic multidecadal variability (AMV), although other mechanisms have a large role, such as the atmospheric stochastic forcing (Clement et al., 2015; Cane et al., 2017) or the changes associated to external forcings (Murphy et al., 2017; Qin et al., 2020).

Most previous studies of the North Atlantic climate variability (e.g., Kerr, 2000; Danabasoglu, 2008; Nigam et al., 2011; Brown et al., 2016; Zhang et al., 2017; Colfescu & Schneider, 2020) mainly focused on periods within 10-70-yr, in agreement with the variability observed in the instrumental period since 1850. Here, we concentrate instead on the centennial to multi-centennial periods. Several paleo-proxy records have suggested the existence of a centennial to multi-centennial variability in the North Atlantic (Nyberg et al. 2002; Sicre et al., 2008) or in the Northern Hemisphere (Mann et al., 1995; Laepple & Huybers, 2013; Ayache et al., 2018). However, the relative significance of internal variability compared to the external forcing from solar irradiance and volcanic aerosol variations remains unknown.

The potential mechanisms for low-frequency variability in the North Atlantic (multidecadal to multi-centennial) remain an open question due to the limited availability of instrumental records. The AMOC observing systems have both short temporal and sparse spatial coverage. Continuous observations of the AMOC conducted by the Rapid Climate Change (RAPID) program only started in 2004 and are confined in the subtropical North Atlantic (Cunningham et al., 2007). Hence, models are needed to explore the low-frequency variability of the AMOC, even if biases in the simulated AMOC and its associated heat transport remain in most general circulation models (GCMs; Zhang et al., 2019; Xu et al., 2019). Variability of the North Atlantic on multidecadal (particularly referring to scale longer than 70 yr hereafter) to multi-centennial scale is found in a number of models. Delworth & Zeng (2012) found connections between the Southern Ocean and the subpolar North Atlantic through the propagation of salinity anomalies in the GFDL CM2.1. Park and Latif (2008) also emphasized in the KCM model the importance of freshwater anomalies from the Southern Ocean, associated with sea ice cover anomalies. Vellinga and Wu (2004) proposed that the subtropical salinity anomaly generated by the AMOC-driven northward shift of the ITCZ was the source of the AMOC oscillations in the model HadCM3. The freshwater anomaly is advected toward the subpolar Atlantic in 5 to 6 decades. On the other hand, some studies argue that the variations come from the Arctic. Jungclaus et al. (2005) suggested that the anomalous export of freshwater from the Arctic center and anomalous circulations in the Nordic Seas were responsible for the 70-80-year variability in the MPI coupled model. A dominant role of freshwater exchanges between the Arctic and North Atlantic regions also appears in other studies (Hawkins and Sutton, 2007; Pardaens et al., 2008; Jahn & Holland, 2013). With an ensemble of perturbed physics based on HadCM3, Jackson and Vellinga (2013) proposed that the salinity anomalies in the deep-water formation sites not only originated in the tropical North Atlantic as described previously in Vellinga and Wu (2004), but also originated in the Arctic Ocean, probably driven by the stochastic sea level pressure.

In the present study, we explore the centennial variability emerging in the North Atlantic in the IPSL (Institut Pierre Simon Laplace) atmosphere-ocean model developed for CMIP6 (Coupled Model Intercomparison Project Phase 6, Eyring et al., 2016). Boucher et al. (2020) identified that in the multi-centennial preindustrial control simulation of this model, both the AMOC and AMV fluctuate with an approximate period of 200-yr. We will show that these oscillations are generated by a slow build-up of freshwater anomalies in the central Arctic when the AMOC is intensified, resulting from reduced sea-ice export. This freshwater is eventually

This article is protected by copyright. All rights reserved.

flushed into the Nordic Seas and the North Atlantic with a delay of 4 to 5 decades, reversing the sign of the AMOC anomalies.

2 Data and methodology

2.1 Model description

IPSL-CM6A-LR is the low resolution (LR) version of the IPSL-CM6A model developed by the IPSL for CMIP6. A complete description of this model is provided in Boucher et al. (2020), and we will focus below on the main characteristics relevant to the investigation of the low-frequency climate variability. The atmospheric component is LMDZ6 and has a resolution of $1.26° \times 2.5°$ and 79 levels in the vertical (up to 1 Pa). The oceanic model NEMO has 75 vertical levels and a nominal resolution of about 1° in the horizontal, refined up to $1/3°$ in the equatorial and polar regions (ORCA1 grid). The sea ice module is LIM3.6 and adopts five sea-ice thickness categories. We use the outputs from a 2000-year pre-industrial control simulation performed for CMIP6. This run follows a 100-yr spin-up and uses pre-industrial land-use and atmospheric concentration of greenhouse gases, aerosols, and stratospheric ozone. A cooling drift exists in this simulation, although it remains small at about 0.2K in 2000 years. This drift was approximated by a quadratic trend, which was removed from all data before analysis.

2.2 Assessment of the Arctic Ocean in the model

To evaluate the simulated salinity and temperature fields in the Arctic and the North Atlantic, we use the World Ocean Atlas 2018 (WOA18) dataset (Locarnini et al., 2018; Zweng et al., 2018) for comparison. In this study, the regions of interest are the Arctic and the North Atlantic (Fig. S1). The Arctic is defined as being enclosed by the Fram, Bering, and Davis straits and the Barents Sea. The location of the four cross-sections is given in Fig. S1. In the top 200m, the simulated Arctic temperature has a good agreement with the WOA18 dataset (Fig. S1d). However, the warm and salty North Atlantic inflow, shown by the ~1°C potential temperature maximum at 400m in WOA (Fig. S1a), is absent in the model. Instead, IPSL-CM6-LR simulates a uniform water mass at ~0.2°C from 300m to 2000m, suggesting either an underestimation of the inflow of Atlantic water or an unrealistic mixing of the North Atlantic inflow with the Arctic deeper water. In addition, the salinity in the top 200m is overestimated in the Arctic, especially in the Eastern Arctic over the shallow continental shelf (Fig.S1c), suggesting an underestimated runoff from the Eurasian continent or a bias resulting from the coarse resolution of the steep continental slope. The same diagnostics in the North Atlantic, from 30°N to the Fram Strait and Barents Sea Opening cross-section, also show that the simulated upper North Atlantic Deep Water is too cold between 300m and 800m (Fig. S1b). This bias is associated with a relatively weak AMOC in IPSL-CM6A-LR, with a mean Atlantic meridional streamfunction at 30°N of 10.8 Sv (from 6.5 Sv to 15.4 Sv), while the deep oceanic convection is underestimated in the Labrador Sea and overestimated in the Nordic Seas (see Boucher et al. 2020). The model also simulates a cold and fresh bias in the subpolar gyre (Fig. S1c and d), as the Gulf Stream and North Atlantic current are not well resolved when using a low oceanic resolution (Wang et al., 2014; Flato et al. 2013).

Figure S2a shows the mean oceanic currents and salinity in the top 150m. The Atlantic water inflow through the Barents Sea is well simulated in the model, while the intensity of the West Spitzbergen Current in the Eastern Fram Strait is underestimated compared to observations (Aksenov et al., 2011). This may contribute to the bias of the simulated Atlantic water in the Arctic, as discussed above. The fresh Beaufort Gyre located in the Canadian Basin is generally present in IPSL-CM6A-LR, but the associated anticyclonic circulation is not fully developed. Besides, the

This article is protected by copyright. All rights reserved.

transpolar drift near 150°E and toward the Fram Strait is shifted west towards the north of the Canadian Archipelago in the Lincoln Sea (Pnyushkov et al., 2015; Petty et al., 2016). This might lead to an overestimation of the current north of Greenland and of the Atlantic inflow penetrating the Beaufort Gyre.

Table 1.Mean freshwater budget in the Arctic Ocean. Reference salinity is 34.8 psu. Transport and fluxes are positive when entering the Arctic. Uncertainty in IPSL-CM6-LR is one standard deviation and is calculated from yearly outputs.

	Freshwater Transport (mSv)					Freshwater fluxes (mSv)	
	Fram Strait	Bering Strait	Barents section	Davis Strait	Total	Runoff	P-E
IPSL-CM6-LR							
Liquid	-32.6±23.3	71.2±15.0	10.6±13.2	-112.8±33.3	-63.5±32.2	108.9±5.6	46.1±5.2
Sea ice	-63.1±14.9	-0.63±4.0	-11.7±5.9	-8.9±3.4			
Observations							
Liquid	-63/-95/-28	57/79	-18	-92		94/102	65/31
Sea ice	-56/-88	3.00	-3.9	-12.9			

To further explore the origin of the broad positive salinity bias in the Arctic, we quantify the freshwater exchanges between the Arctic and the Atlantic. Freshwater can exit the Arctic in liquid form or as sea ice. The liquid freshwater transport is computed on the four cross-sections previously identified, from the monthly mass transport and salinity fields. The mass transport used includes resolved and parameterized advective transport. As the mean Arctic salinity in our model and observations is about 34.8 (Fig. S1), we take 34.8 as reference salinity. These sections are along the ocean grid to facilitate the calculation. We use the sea-ice-mass transports provided by the CMIP6 outputs, at slightly different locations (given in Notz et al. 2016) from that shown in Fig. S1, but still through the same passages. We assume a constant sea-ice salinity of 7.2 psu to compute the freshwater proportion in the sea-ice mass transport. Table 1 compares the freshwater transport in IPSL-CM6A-LR to various observational estimates (summarized by Lique et al., 2009). The liquid export of Arctic freshwater occurs mainly through the Davis and Fram Straits, and the model underestimates the export through Fram to some extent. The freshwater input from the Bering Strait is realistic and leads to a relatively fresher Beaufort Gyre and a salinity gradient in the Arctic from the Pacific sector to the Atlantic sector (Fig. S2a). The liquid freshwater transport at the Barents Sea Opening is smaller compared with the other three sections. It has a sign opposite to that of observations, with considerable uncertainty, which possibly leads to the underestimation of salinity in the Arctic between 200m-600m (Fig.S1a). The flux due to precipitation minus evaporation (P-E) is underestimated, which may explain the occurrence of the positive surface salinity bias in comparison with WOA dataset. Nevertheless, the freshening caused by the runoff seems to be well simulated and results in the salinity minimum apparent in the coastal seas of the eastern Arctic (Fig. S2a). Therefore, the large positive bias in this region is more likely to result from the bottom topography (Fig. S1c). Lastly, an overwhelming majority of the sea ice export is realized through the Fram Strait, and the model simulates well this export.

This article is protected by copyright. All rights reserved.

2.3 Statistical Methods

2.3.1 Empirical orthogonal function and low frequency component analysis

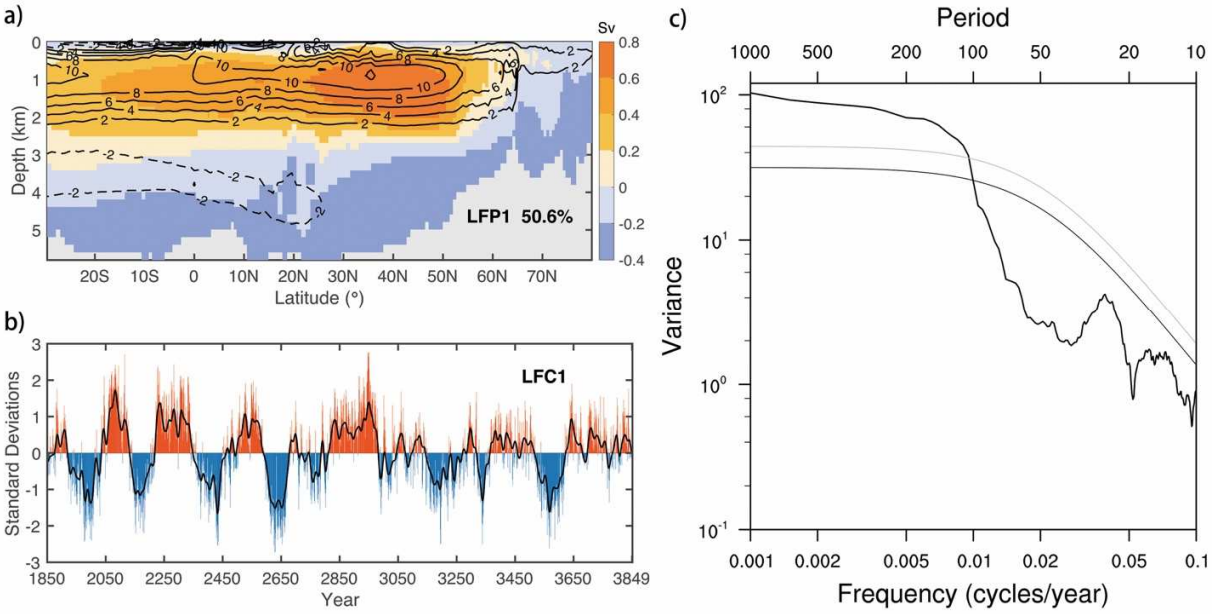

Figure 1. (a) First Low-frequency pattern (LFP1) of the meridional streamfunction in the Atlantic basin from 30°S to 80°N (colors) and the climatological mean meridional streamfunction (contours), in Sv. The streamfunction is positive for clockwise rotation. LFP1 accounts for 50.6% of the low frequency variance sampled by the first 8 empirical orthogonal functions. (b) (Colors) standardized first Low frequency component (LFC1). The black line shows the maximum of the Atlantic meridional streamfunction at 30°N, after applying a third-order Butterworth lowpass filter with a cutoff period of 20-yr. (c) The variance-frequency spectrum of LFC1 (in black). The best-fit first-order Markov red noise spectrum (lower gray curve) and its 95% (upper gray curve) confidence bounds are also indicated.

To characterize the centennial variability, we first compute the empirical orthogonal functions (EOF) of the Atlantic yearly meridional streamfunction from 30°S to 80°N, after weighting the data by the square root of the grid cell thickness. Hereafter, the principal components (PC) time-series are standardized, while the EOFs shown are the regressions onto the PCs. The resulting first EOF (Fig. S3, left) explains 21% of the variance and has largest loadings in the Tropics between 10°S and 10°N. The corresponding first PC shows some centennial to multi-centennial variability, but it also includes some variations with a period smaller than 10-yr. Conversely, the second EOF explains 16% of the variance and has large loadings between 40°N and 50°N. The associated second PC also shows a clearer centennial to multi-centennial variability (Fig. S3, right). The two PCs are positively correlated over a broad range of non-zero lags (with PC2 leading by a decade); this illustrates that standard EOF analysis, designed to maximize the variance, fails in our case to isolate a multi-centennial variability with large meridional coherence. Therefore, we use instead a low frequency component analysis (LFCA). The LFCA looks for the

This article is protected by copyright. All rights reserved.

linear combination of the EOFs that maximizes the ratio of low frequency to total variance (Wills et al., 2018). The LFCA then provides the spatial pattern, called low frequency pattern (LFP), that explains most of the low-frequency variance. The associated time series, called low frequency component (LFC), is found by projecting the original unfiltered data onto the LFP. Here, we apply the LFCA using the first 8 EOFs, explaining 73.8% of the total variance, and the low-frequency time series are calculated using a third-order Butterworth filter with a 20-yr cutoff period. The first LFP then explains 50.6% of the low frequency variance (Fig. 1, top) and is a meridional coherent overturning cell extending from 30°S to 80°N, with a typical variability of 0.8 Sv between 30°N-50°N. The associated LFC1 shows a clear multi-centennial variability. Using 10-yr as the cutoff period in the Butterworth filter applied does not lead to significant differences. In the following, LFC1 is used as an index of centennial AMOC fluctuations.

2.3.2 Regression and significance test

The regression of various fields onto the LFC1 AMOC index is used to investigate the mechanisms of the centennial to multi-centennial variability. The statistical significance of the correlated time series is estimated by a nonparametric method (Ebisuzaki, 1997). We create a large number of surrogate time series with the same power spectra as the AMOC LFC1 time series but with randomized phases in Fourier space. The original correlation between the AMOC index and the field of interest is compared to the distribution of correlations with the surrogate time series. The statistical significance level is the fraction of surrogate time series with a larger correlation than the actual value. 100 surrogate timeseries are used in our case to estimate the significance. To ease the calculation of the regression maps, we convert the annual mean data into decadal time series, replacing every 10-yr blocks by their time average. Only few differences were found when using annual mean data.

In the following text, the sign convention is that the AMOC leading the regressed fields is positive. For instance, "at lag -10 yr" means that the AMOC lags by 10 years.

Accepted Article

This article is protected by copyright. All rights reserved.

3 Results

3.1 Role of salinity

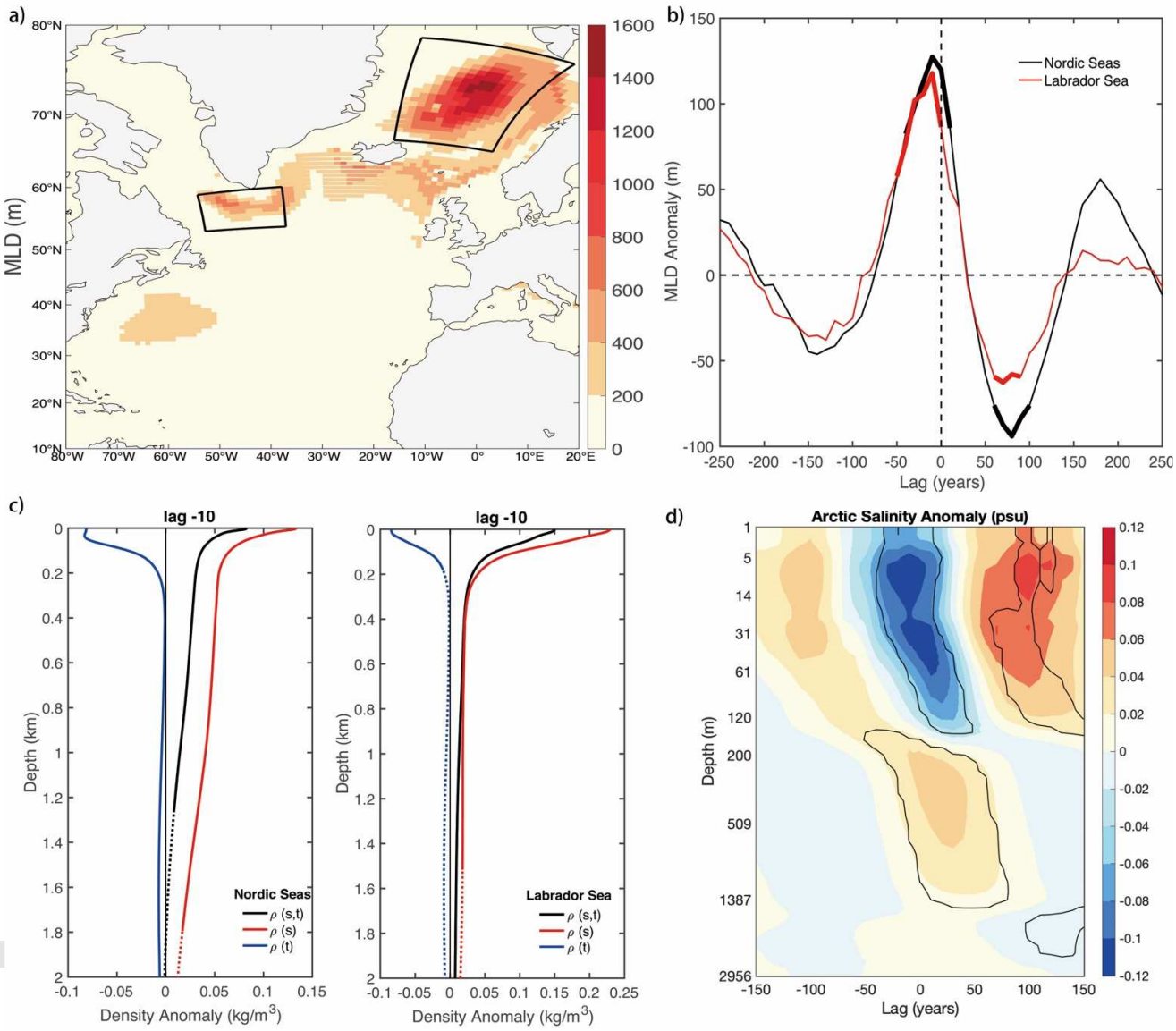

Figure 2. (a) Mean mixed layer depth (MLD), in m, in February, March and April (FMA). Two convective sites: the Nordic Seas (the upper one) and Labrador Sea (the lower one) are outlined with black boxes. (b) Lagged regression of FMA MLD onto AMOC LFC1. The lag is positive when the AMOC leads. The thick lines indicate significance level below 5%. (c) Density anomaly (in black), in kg m^{-3}, regressed onto AMOC when the AMOC lags by 10 yr, in the Nordic Seas and Labrador Sea convection sites. The density anomaly $\rho(s,t)$ caused by salinity anomaly $\rho(s)$ or temperature anomaly $\rho(t)$ is given in red and blue, respectively. Full (dashed) lines indicate the significance level below (above) 5%. (d) Vertical section of the lagged regression of the Arctic-wide averaged salinity. Black lines indicate significance level of 5%. The vertical scale is proportional to the mean size of the model vertical levels.

This article is protected by copyright. All rights reserved.

As previously illustrated by the LFCA, a clear multi-centennial variability is found in LFC1 (Fig.1). For comparison, the black line in Fig.1b is the standardized time series of maximum AMOC streamfunction at $30°N$ smoothed with a lowpass filter using 20-yr as cutoff period. We find that LFC1 captures many characteristics of the raw AMOC time series. As noted in Boucher et al. (2020), the first 1000-yr of the pre-industrial control run shows some variability with an approximate period of 200-yr, but the last 1000-yr shows a less regular variability. A spectrum analysis of LFC1(Fig.1c) indeed shows a broad maximum emerging for periods longer than 100 years, without any clear peak. We also note a small peak at 30-yr, which could be similar to the variability produced in the previous version of the IPSL model, IPSL-CM5A-LR (Escudier et al., 2013; Ortega et al., 2015). But this peak has less variance than the multi-centennial variability and remains below the fitted red noise spectrum.

In IPSL-CM6A-LR, the mean mixed layer depth (MLD) in February-March-April (FMA) depicts one dominant deep-water formation site in the Nordic seas, with mean MLD of ~1400m; and a smaller one in the Labrador Sea (Fig. 2a), with mean MLD of ~600m. The lagged regression of the FMA MLD in these two sites onto LFC1 reaches a maximum anomaly of ~120m at both sites at lag -10 yr (Fig. 2b). To figure out the relative importance of salinity and temperature anomalies in driving the convection at those two sites, we calculate the density anomalies caused by anomalous salinity and temperature, while keeping the other field as its mean value. The results show that the upper (0-200m) density anomalies are dominated by salinity anomalies and slightly balanced by temperature's impacts. The effect of temperature also decreases with depth and becomes negligible below 200m (Fig. 2c). The deepening of the MLD preceding the AMOC is therefore mainly induced by salinity anomalies. We also note that these salinity-driven density anomalies occur almost simultaneously in the Nordic and Labrador Seas (Fig. 2b).

Accepted Article

This article is protected by copyright. All rights reserved.

Accepted Article

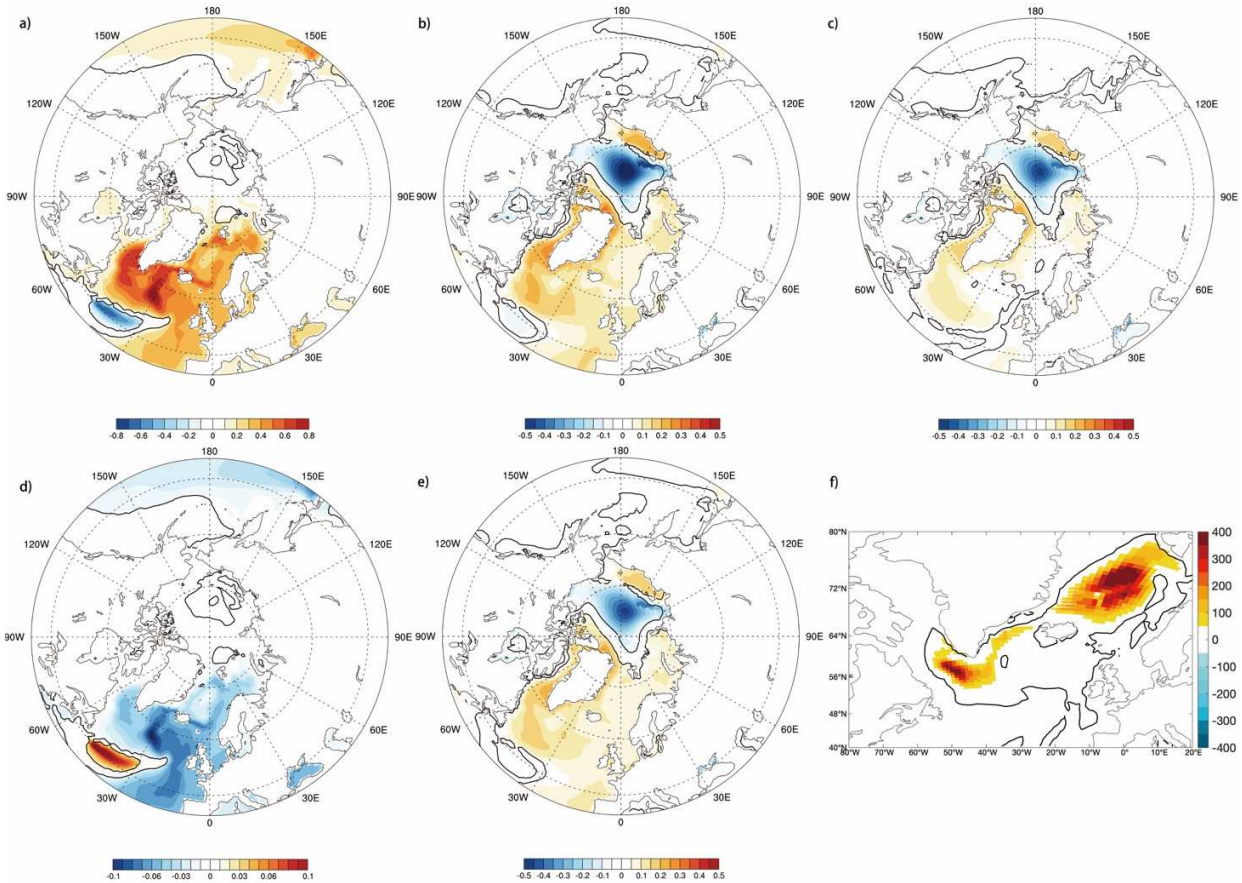

Figure 3. Oceanic fields regressed onto AMOC LFC1 when the AMOC lags by 10-yr. (a) Regressed temperature (in ℃), (b) salinity (in psu) and (c) density (in kg m^{-3}) in the top 150m. (d) Thermal and (e) haline components (in kg m^{-3}) contributing to the density anomaly in (c). Note the difference in color scale for (d) when compared to (c) or (e). (f) Regressed MLD in FMA (in m). The black lines in (a)-(f) indicate the significance level at 5%. The red lines in (a) indicate the locations of transects and the blue points indicate each section's starting position.

Figure 3 (a) - (c) show maps of temperature, salinity, and density anomalies in the top 150m at lag -10 yr, corresponding to the deepest MLD. In the subpolar gyre, the warming and salinization pattern is coherent with that found in other studies of low frequency Atlantic variations (e.g., Drews & Greatbatch, 2017; Roberts et al., 2013), with a southward extension of the subpolar gyre. The similarity between the density and salinity anomaly patterns clearly reveals the solid impact of salinity on density. The corresponding thermal and haline components of the density anomalies, shown in Figs. 3 (d) and (e), further illustrate that the Arctic density anomaly is almost entirely determined by the abnormal salinity. The temperature slightly influences the eastern part of the Nordic seas and subpolar gyre since the Atlantic Ocean warms when the AMOC is strong. But its impact is smaller than that of salinity. Despite a smaller density anomaly in the Nordic Seas compared to the Labrador Sea, the anomalous MLD at these two sites are of comparable amplitudes (Fig. 3f), and even the Nordic Seas anomalies have a broader extent. This may be linked to deeper mean MLD in the Nordic Seas.

Farther from the convection sites, we find a sizeable negative salinity anomaly in the Central Arctic, contrasting with the positive salinity anomalies located around Greenland and in the East Siberian Sea (Fig. 3b). The regression of the basin-averaged salinity shows that this Central Arctic freshwater anomaly is located above 200m and is present from lag -40 yr to 40 yr

This article is protected by copyright. All rights reserved.

(Fig. 2d). This fresh anomaly is balanced by a smaller positive salinity anomaly between 200m and 1400m. As the top ~150 m presents an opposite salinity anomaly with the underlying ocean, in the following, we use the mean of the upper 150m to characterize the Arctic salinity anomalies.

To better illustrate the salinity anomalies in the Arctic Ocean, we regress the salinity onto AMOC LFC1 in a cross-section across the Arctic from northern Greenland to the coast of northern Siberia (see Fig. 3a for location). At lag -40 yr, the AMOC strengthens from the neutral state. While salty anomalies are present at the north coast of Greenland, a fresh anomaly occupies the top 60m in the rest of the Arctic. Its structure suggests both a deepening and poleward extension of the surface freshwater pool found off the Siberian coast. At lag -10 yr (Fig. 4b), corresponding to a strong AMOC, this initial fresh anomaly has grown and extended towards Greenland, where the positive anomalies have decreased. Small positive salinity anomalies have appeared at the continental slope of northern Siberia, and below 180m.

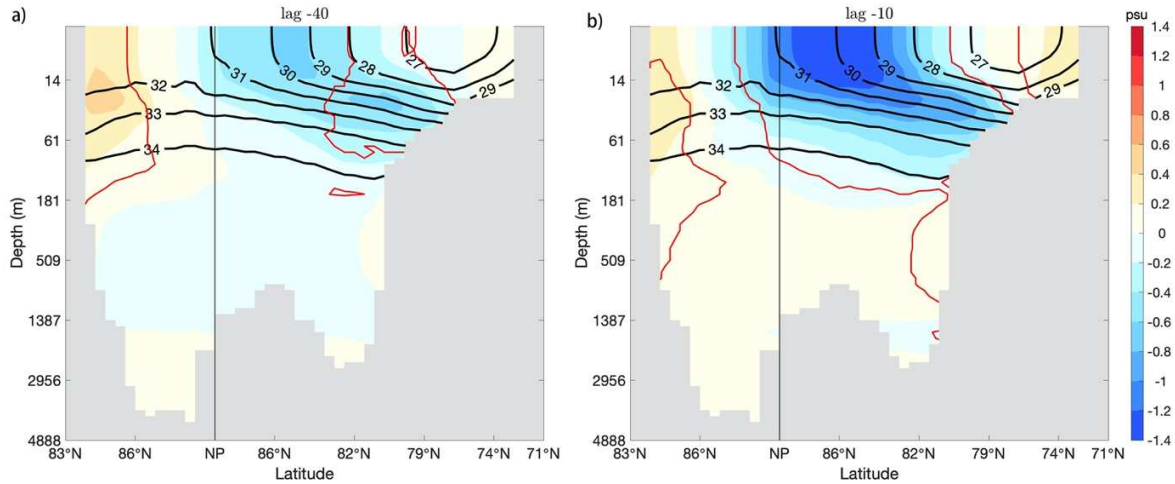

Figure 4. Salinity, in psu at the Arctic cross-section, from (left) Northern Greenland to (right) the East Siberian Sea. (a) Anomalous (in colors) and mean (in black contours) salinity along the section, leading AMOC by 40-yr. (b) Same as (a) but for leading AMOC by 10-yr. Red contours indicate the significance level at 5%. The vertical scale is proportional to the mean size of the model vertical levels.

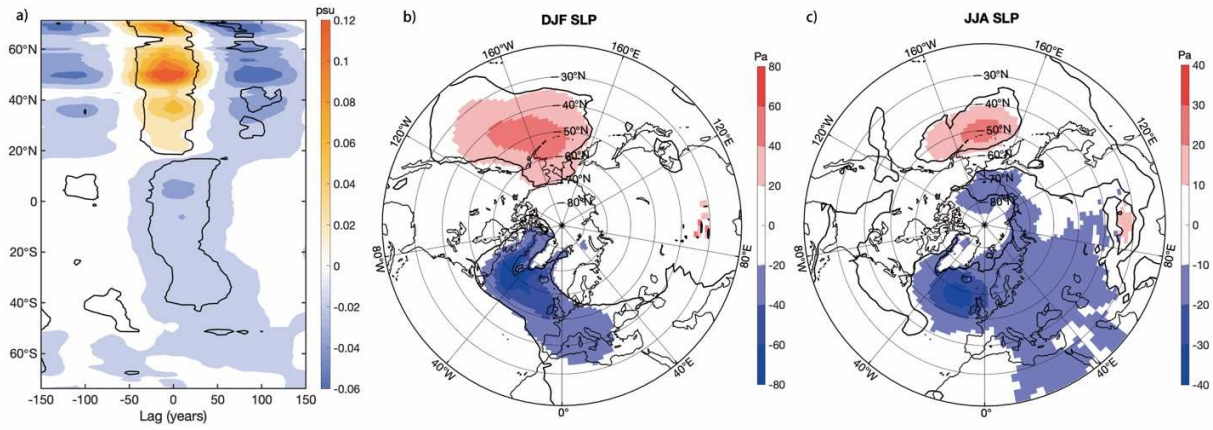

Figure 5. (a) Zonal-mean salinity anomalies in the Atlantic basin regressed onto AMOC LFC1 (in colors). Black lines illustrate the significance level at 5%. (b) Anomalous sea level pressure (SLP), in Pa, in December, January, February (DJF) and (c) June, July and August (JJA) regressed onto AMOC LFC1, when the AMOC lags by 10-yr.

This article is protected by copyright. All rights reserved.

Before investigating the link between the Arctic and North Atlantic salinity anomalies, we briefly inspect other possible drivers, such as atmospheric forcing or the propagation of salinity anomalies from the tropics (e.g., Vellinga and Wu, 2004) or the Southern Ocean (e.g., Delworth & Zeng, 2012). To characterize the variations of anomalous salinity in the Atlantic Ocean, we show the Hovmöller diagram of the regression of the Atlantic zonal-mean salinity (0-150m) onto LFC1 (Fig. 5a). Indeed, the positive salinity anomalies occurring in the North Atlantic between 20°N and 60°N are associated with fresh anomalies between the equator and 15°N, as noticed by Vellinga and Wu (2004). However, these tropical fresh anomalies do not seem to propagate northward. Furthermore, few anomalies appear south of 40°S in the Southern Ocean, unlike previous studies (Delworth and Zeng, 2012; Park and Latif, 2008). The positive salinity anomalies in the middle-latitude North Atlantic seem instead to follow positive anomalies North of 60°N. Even if cause and effect cannot be fully distinguished, this suggests a stable linkage between the Arctic Ocean and the salinity anomalies driving the AMOC centennial variability. Finally, we investigate the potential role of the atmospheric forcing, showing the regression of the sea level pressure (SLP) onto AMOC LFC1 when the SLP leads the AMOC LFC1 by 10-yr (Fig.5b and c). The SLP decreases over the subpolar Atlantic during a strong AMOC, but the magnitude of the anomalies is small: about 40 Pa at maximum. As we will show in the following, the associated geopotential height anomalies at higher altitudes have the opposite sign. Such a baroclinic structure contrasts with the barotropic modes of atmospheric variability previously identified as driving the AMOC (Eden and Willebrand, 2001; Hakkinen et al., 2011). Moreover, the SLP anomalies over the Arctic are not statistically significant, nor are surface wind anomalies (not shown). Therefore, it is likely that the SLP anomalies and the tropical salinity anomalies are the results of the strong AMOC, not the cause of the AMOC changes. In the following, we will investigate how salinity anomalies coming from the Arctic regulate the AMOC.

Accepted Article

This article is protected by copyright. All rights reserved.

3.2 Life cycle of the salinity anomalies

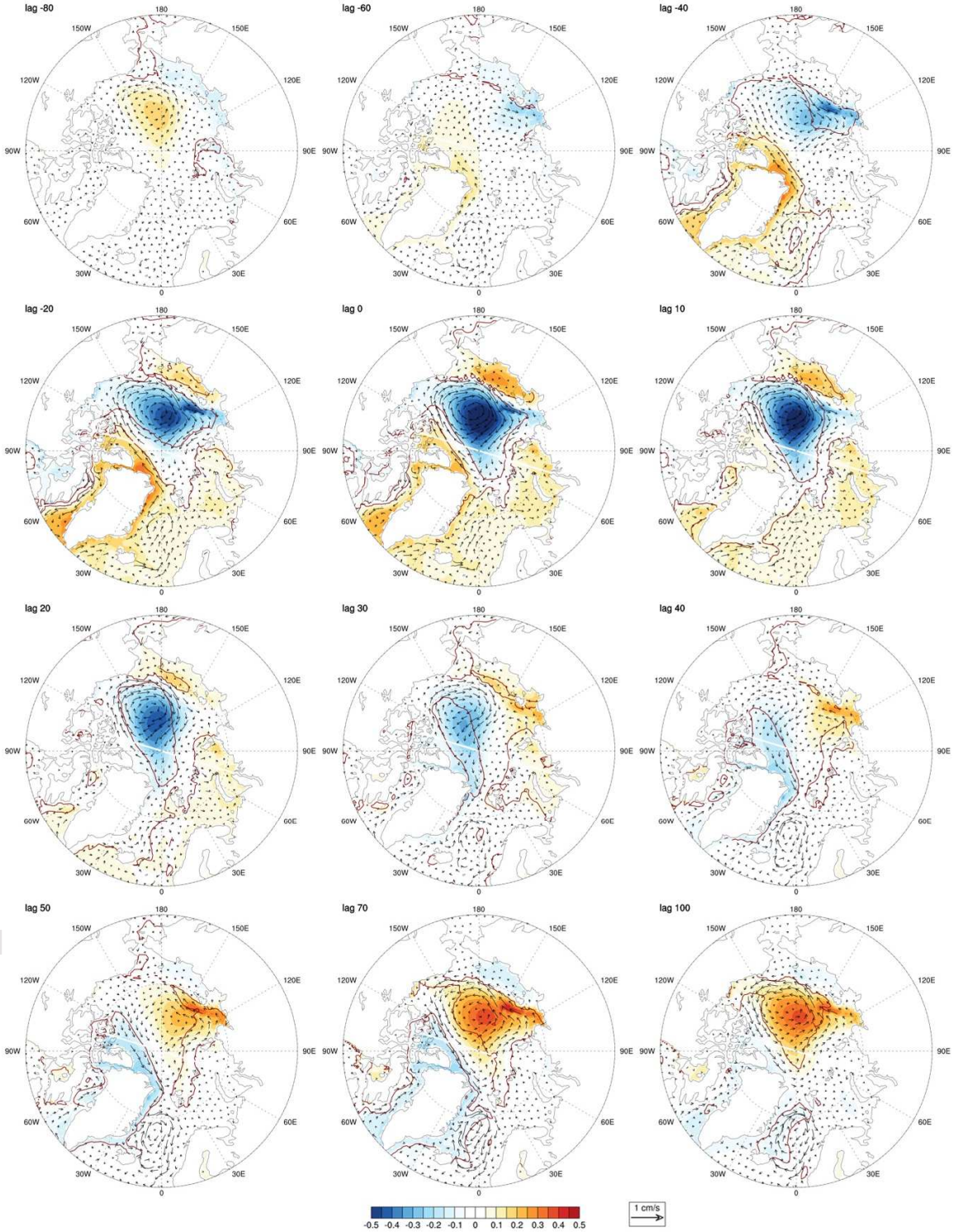

Figure 6. Regression onto AMOC LFC1 of the top 150m salinity (colors), in psu, and currents (arrow), in cm s^{-1}, onto AMOC LFC1. Red contours indicate the significance level at 5% for the salinity regression. The lag is positive when the AMOC leads.

Accepted Article

This article is protected by copyright. All rights reserved.

To investigate the propagation of salinity anomalies and understand the associated mechanisms, figure 6 shows lagged regression maps of the top 150m salinity and currents in the Arctic. From lags -80-yr to -60-yr, positive salinity anomalies occur in the Arctic center then propagate to the coast of Greenland, especially the Lincoln Sea and the Fram Strait. Minor negative anomalies appear in the East Siberian and the Laptev Seas. However, most of those anomalies are not significant at the 5% level. By lag -40 yr, the salty anomaly around Greenland has grown and spread into the Nordic Seas, while a fresh anomaly appeared in the Central Arctic. These salinity anomalies are associated with an anomalous anticyclonic circulation in the central Arctic, and a cyclonic one around Greenland, with weakened West Greenland Current (WGC) in the Baffin Bay and East Greenland Current (EGC) through the Fram Strait, closed by a westward anomalous current north of Greenland.

From lags -20-yr to 0-yr, the AMOC gradually reaches its maximum value. The fresh anomaly in Central Arctic intensifies to about -0.5 psu. The gradual accumulation of freshwater leads to the reinforcement of the associated anticyclonic geostrophic flow. This anomalous circulation likely contributes in turn to maintaining this fresh anomaly in the central Arctic instead of it flushing through Fram Strait, as observed in the recent decades (Proshutinsky et al., 2009; Petty et al., 2016). Both the abnormal freshwater pool and anticyclonic circulation peak together with the AMOC (lag 0-yr), while the salty anomaly around Greenland has started to decrease.

When the AMOC leads by 10-yr, the Central Arctic freshwater finally reaches the Lincoln Sea and quickly spreads around Greenland. The accumulated freshwater is then gradually exported toward the Atlantic Ocean through the Fram straight from lag 20-yr to lag 40-yr, presumably through advection by the mean current, as well as by a stronger southward WGC. We notice that the negative salinity anomaly decays before exiting the Arctic (lag 30), probably due to the advection of the positive anomalies from the Eastern coastal Arctic to the Central Arctic (Fig 4b). When the freshwater has completely disappeared from the Central Arctic (lag 40-yr to lag 70-yr), an anomalous anticyclonic circulation sets up around Greenland, together with negative salinity anomalies. Simultaneously, a positive salinity anomaly initially located in the East Siberian and Laptev Seas at lag 30-yr builds up and expands into the Central Arctic from lag 30-yr to lag 70-yr. This salty anomaly is associated with an anomalous cyclonic flow. The pattern shown at lag 70-yr is of the opposite sign when compared to that found during the strong AMOC (lag 0-yr). We can note during this cycle alternating near-surface salinity anomalies between the Central Arctic and at the Greenland coasts, with positive anomalies around Greenland leading the AMOC by 40 to 0-yr and negative anomalies lagging the AMOC by 40 to 70 yr, while the central Arctic anomalies are more in phase. This relatively uniform distribution around Greenland could result from a fast adjustment of salinity and current anomalies trapped around Greenland, associated with opposite anomalous EGC and WGC.

To trace the source of the surface freshwater, we inspect the variations of sea ice thickness (Fig 7a), volume (Fig. 7b, red line), and area (Fig. 7b, black line). The reduction of sea ice in all aspects is simultaneous with the AMOC. This is consistent with a sea ice loss associated with the persistent warming linked to the increased northward oceanic heat transport, as previously found in models simulating a substantial multi-decadal Atlantic variability with a period larger than 40-yr (Frankcombe et al., 2010; Mahajan et al., 2011). As we discussed before, the atmospheric circulation above the Arctic Ocean is not significantly modified by the multi-centennial variability, while the oceanic anticyclonic oceanic currents anomalies increase at lag -10-yr (Fig. 6). This results in a clockwise sea-ice velocity anomaly (see arrows in Fig. 7a).

Accepted Article

This article is protected by copyright. All rights reserved.

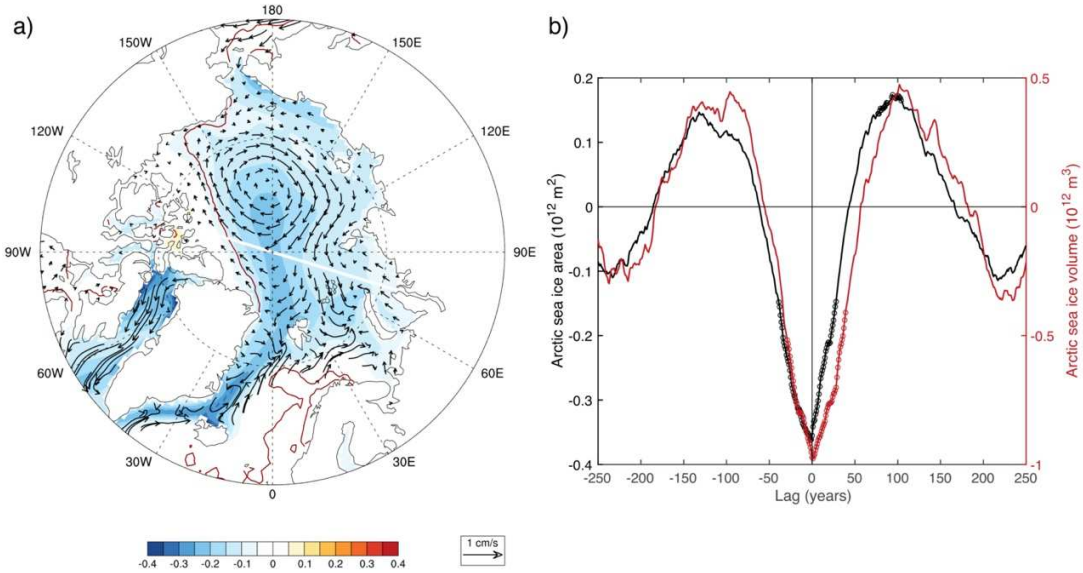

Figure 7. (a) Sea ice thickness in March (in colors), in m, and sea ice velocity (in black curved arrows), in $cm \cdot s^{-1}$,when the AMOC lags by 10 yr. Red contours indicate the significance level at 5% of sea ice thickness. (b) The lagged regression of Arctic sea ice extent (in black line), in $10^{12} m^2$, and the lagged regression of equivalent freshwater of Arctic sea ice volume (in red line), in $10^{12} m^3$. The lag is positive when the AMOC leads. Circles indicate significance level below 5%.

In summary, the anomalous salinity anomalies located in the central Arctic grow gradually with the AMOC, associated with anomalous oceanic currents and sea-ice velocity. Conversely, the main convection sites located in the Nordic and Labrador Seas show salinity and density anomalies more linked to large salinity anomalies forming all around Greenland, that lead the AMOC. These anomalies around Greenland in turn result from the delayed propagation of the anomalies located over the Arctic.

3.3 Source of salinity anomalies

To understand the freshwater exchanges between the Arctic and the North Atlantic, we quantify the liquid freshwater and sea-ice transports across the boundaries of the Arctic, as well as the contribution from the sea ice melting/freezing and surface fluxes due to runoff and precipitation minus evaporation (see section 2.2 for details).

Figure 8a reveals that in phase with a strong AMOC (and a maximum accumulated freshwater in the top 150m of the Arctic), there is a large compensation between a freshwater input from sea-ice and surface fluxes (Fig. 8a, black line), and an export by oceanic transport through the straits (Fig. 8a, red line). Among the different contributors to the surface and freshwater fluxes, sea-ice is by far the largest (~9 mSv at lag 0; Fig. 8b, red line). Increased runoff (~1.5 mSv at lag 0) also contributes marginally to the positive surface input. The impact of precipitation and evaporation is negligible (Fig. 8b, orange line). As we will show in the following subsection, the strong AMOC-driven heat transport warms the Northern Hemisphere high latitudes, especially in the lower troposphere in winter over the Arctic (up to ~1.5°C near the surface). This warming is almost simultaneous with the AMOC due to the fast response of the atmosphere, and leads to sea-ice melt all over the Arctic – possibly with some feedbacks. In addition, sea ice export decreases (~5.5 mSv at lag 0; Fig.8d, black line), in line with the decreased volume and weaker currents,

This article is protected by copyright. All rights reserved.

mostly at the Fram Strait (~4.5 mSv Fig.8d, red line) with a small contribution from the Barents Sea (~1.5 mSv at lag 0; Fig.8d, blue line).

To better understand the oceanic freshwater transport, we also detail in Fig. 8c the oceanic transport at each cross-section delimiting the Arctic boundaries. Anomalous transports at the Fram and Davis Straits precede the AMOC by 30 to 40 yr. They are opposite in sign and balance each other to a large extent, with a slightly larger magnitude at Davis (Fig. 8c). These transports are consistent with the cyclonic (anticyclonic) circulation and positive (negative) salinity anomalies trapped around Greenland at lag -40-yr (50-yr), as illustrated in Fig. 6. The total oceanic transport is however in phase with the AMOC (Fig. 8c, black line) and is mainly driven by the saltier Atlantic inflow through the Barents Sea (Fig. 8c, blue line).

The oceanic transport anomalies are further decomposed into the advection of salinity anomalies by the mean current, and the anomalous advection of the mean salinity (Fig. 8c). Both contributions are equally important at the Fram Strait (Fig. 8c, dashed and dotted black lines). The current anomalies dominate at the Davis Strait, and the mean advection of anomalous salinity at the Barents Sea opening.

In order to link these freshwater fluxes with the salinity anomalies, we also compute a simple integrated freshwater budget:

$$\Delta FWC = \int_{t\prime=0}^{t'=t} F_S dt' + \int_{t\prime=0}^{t'=t} F_{Oce} dt' + R \qquad (1)$$

Where F_S denotes the surface and sea-ice freshwater fluxes, and F_{Oce} is the total freshwater fluxes at the straits. ΔFWC is the anomaly of Arctic-integrated freshwater content (FWC). R is a small residue due to the off-line calculation of freshwater transports from monthly outputs. The regression of the terms of Eq. (1) shows that the total Arctic FWC (Fig. 8a, solid black line) continuously decreases from lag -70 to 50 yr, and is a residual of a large cancellation between the two terms on the right-hand side of Eq. (1). The oceanic transport, dominated by the inflow of North Atlantic water through Barents (Fig. 8e, red line), decreases the total Arctic FWC (Fig. 8e, solid black line), resulting in the subsurface positive salty anomalies found below 150m in Fig. 2d or Fig. 4b. Meanwhile, the surface and especially sea-ice fluxes (Fig. 8e, blue line) bring freshwater to the surface, damping the total FWC variations. Although these two terms thus largely cancel each other on average, their impacts on the vertical structure differ, resulting in opposite salinity anomalies in the surface layer and at depth (Fig. 2d). Indeed, the FWC anomaly restricted to the top 150m (Fig. 8e, dashed black line) is positive in phase with a strong AMOC or with a short lag, consistent with the surface freshwater input and with the salinity anomalies shown in Fig. 6. The results suggest that the changes of the accumulated oceanic transport dominate the total and deep FWC anomalies while the surface freshwater fluxes dominate the near-surface FWC, with a contribution from transport anomalies.

Lastly, we compare the FWC variation in the top 150m (Fig. 8f, black line) to the accumulated contribution from cross-neutral diffusion (Fig. 8f, red line). The impact of diffusion is negligible. The internal wave-driven vertical mixing scheme produces low mixing in the polar region (de Lavergne et al., 2015), which is consistent with the little role played by the diffusion in IPSL-CM6A-LR.

This article is protected by copyright. All rights reserved.

Accepted Article

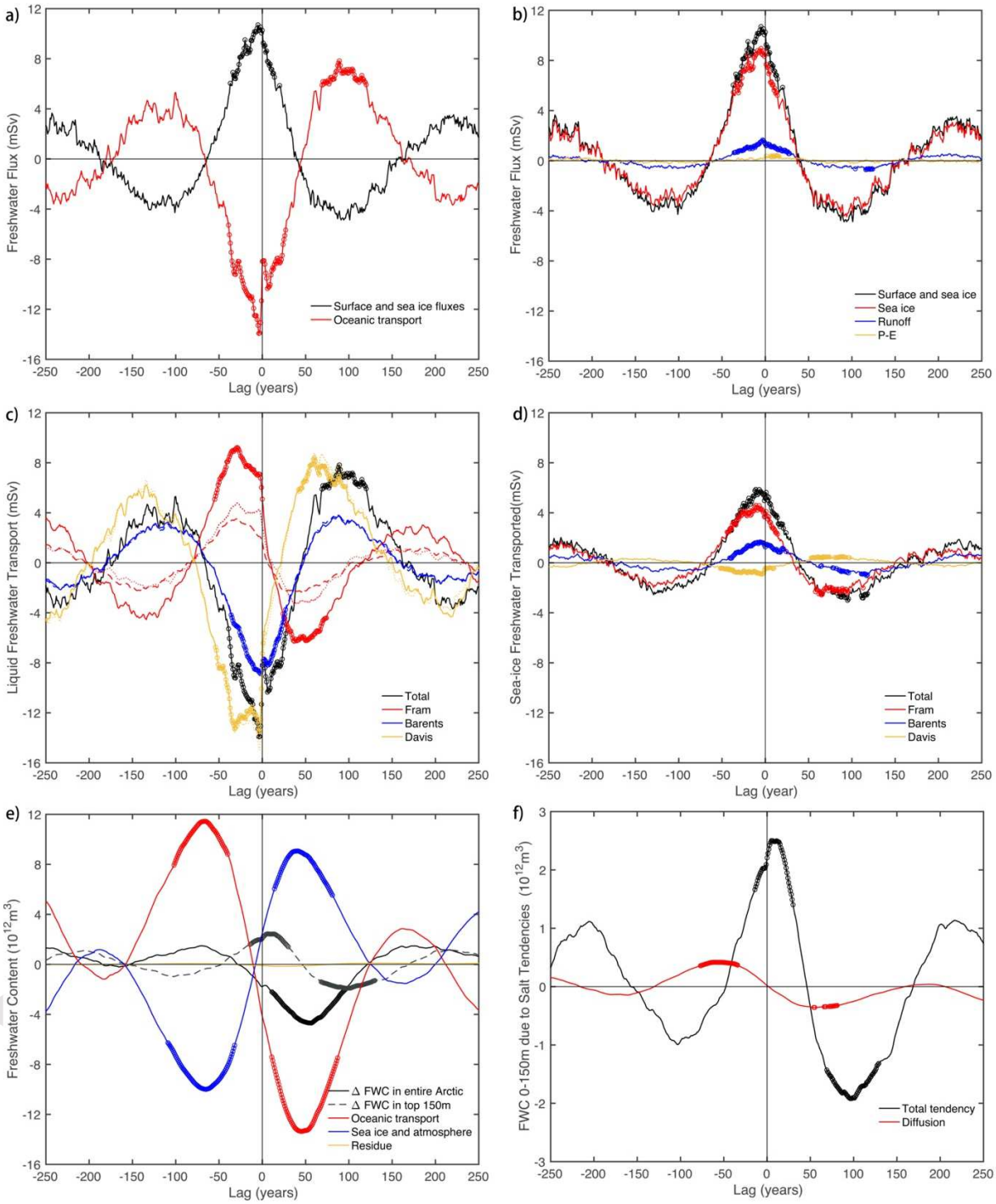

Figure 8. Freshwater content (FWC), in $10^{12}m^3$, and fluxes, in mSv, regressed onto AMOC LFC1 in the Arctic ocean. (a) Regression of the freshwater flux into the Arctic caused by surface and sea-ice thermodynamics fluxes (black line) and liquid freshwater fluxes (red line). (b) Regression of the surface and sea-ice fluxes (black line), sea-ice only flux (red line), the precipitation and evaporation (orange line) and runoff (blue line). (c) Regression of the total liquid freshwater transport (black line) and individual freshwater transport at each section: Fram (red lines), Davis (orange lines) and Barents (blue lines). Solid lines indicate FW transport anomalies; dashed lines represent anomalies caused by mean currents transporting salinity anomalies; dotted lines are

This article is protected by copyright. All rights reserved.

anomalies due to mean salinity transported by anomalous currents. (d) Regression of freshwater flux due to sea ice export in total (black line) and through each passage Fram (red line), Davis (blue line) Straits and Barents Sea Opening (orange line). (e) Regression of the Arctic Ocean FWC variation (solid black line) and FWC variation of the top 150m (dashed black line), and corresponding variation due to accumulated oceanic transport (red line) and freshwater fluxes including sea-ice thermodynamics and surface fluxes (solid blue line) and residual (orange line). (f) Regression of the FWC variation in the top 150m (black line), and contribution from cross-neutral diffusion (red line). In (a) – (f), the significance level below 5% is shown in circles.

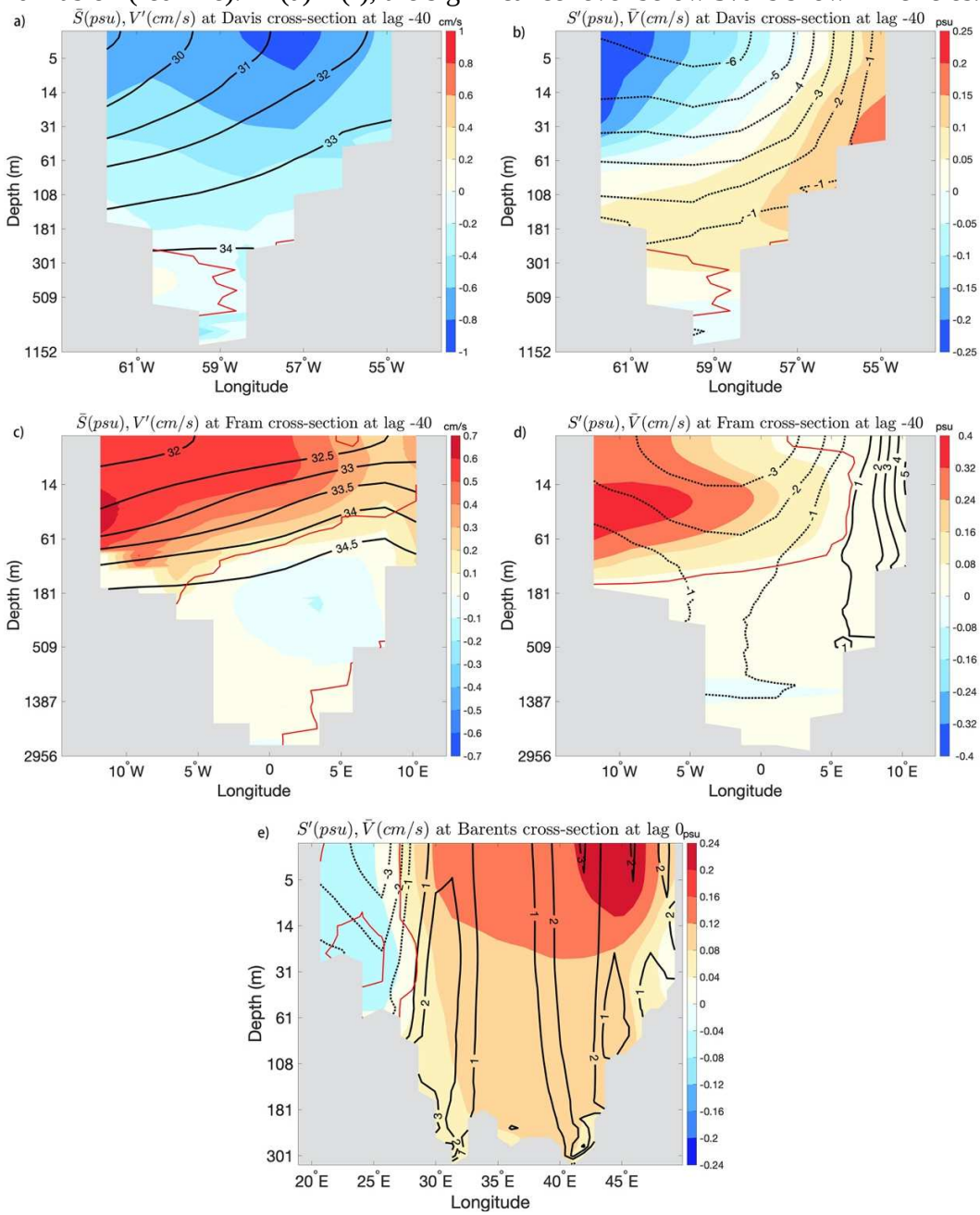

Figure 9. Salinity, in psu, and cross-section current, in $cm \cdot s^{-1}$at the Davis and Fram straits and Barents Sea Opening. (a) and (c) show the mean salinity (in black contours) and anomalous currents (in colors); (b), (d) and (e) show the mean currents (in black contours) and anomalous

This article is protected by copyright. All rights reserved.

salinity (in colors). Note that the depth axis and scale in each plot is different. Red lines indicate the significance level at 5%.

The salinity and current at the three main boundaries of the Arctic Ocean are shown in Fig. 9, at the lags when the respective transport anomalies peak (preceding the AMOC by 40-yr for Fram and Davis, lag 0 for Barents Sea Opening). At Fram Strait, salty anomalies (largest above the halocline) and a weaker EGC appear near the Greenland coast (Fig 9 c, d). These changes are in thermal wind balance, and both act to reduce the freshwater export from the Arctic with a similar magnitude (Fig. 8d, dashed and dotted black lines). The Davis Strait shows anomalous southward flow, consistent with the anomalous cyclonic circulation around Greenland. The salinity anomalies are more complicated, with salty anomalies near Greenland and fresh ones on the other side (Fig. 9b). They correspond to outflow of saltier water from the Lincoln Sea through the Nares Strait and of fresher water from the Beaufort Sea through the Barrow Strait. These opposite salinity anomalies compensate, so the changes of current velocity transporting climatological mean freshwater southward dominate. In the Barents Sea, during strong AMOC conditions (lag 0-yr), the smaller northward freshwater transport is mainly caused by an increase of the salinity of the water entering the Arctic where the mean current is oriented northward (Fig. 9e). This saltier Atlantic inflow enters the Arctic through the Barents Sea Opening and propagates below the halocline toward the Eastern Arctic (Fig. 4b).

Next, we will evaluate the global impacts of the North Atlantic multi-centennial variability.

Accepted Article

This article is protected by copyright. All rights reserved.

3.4 Climate Impacts of the multi-centennial variability

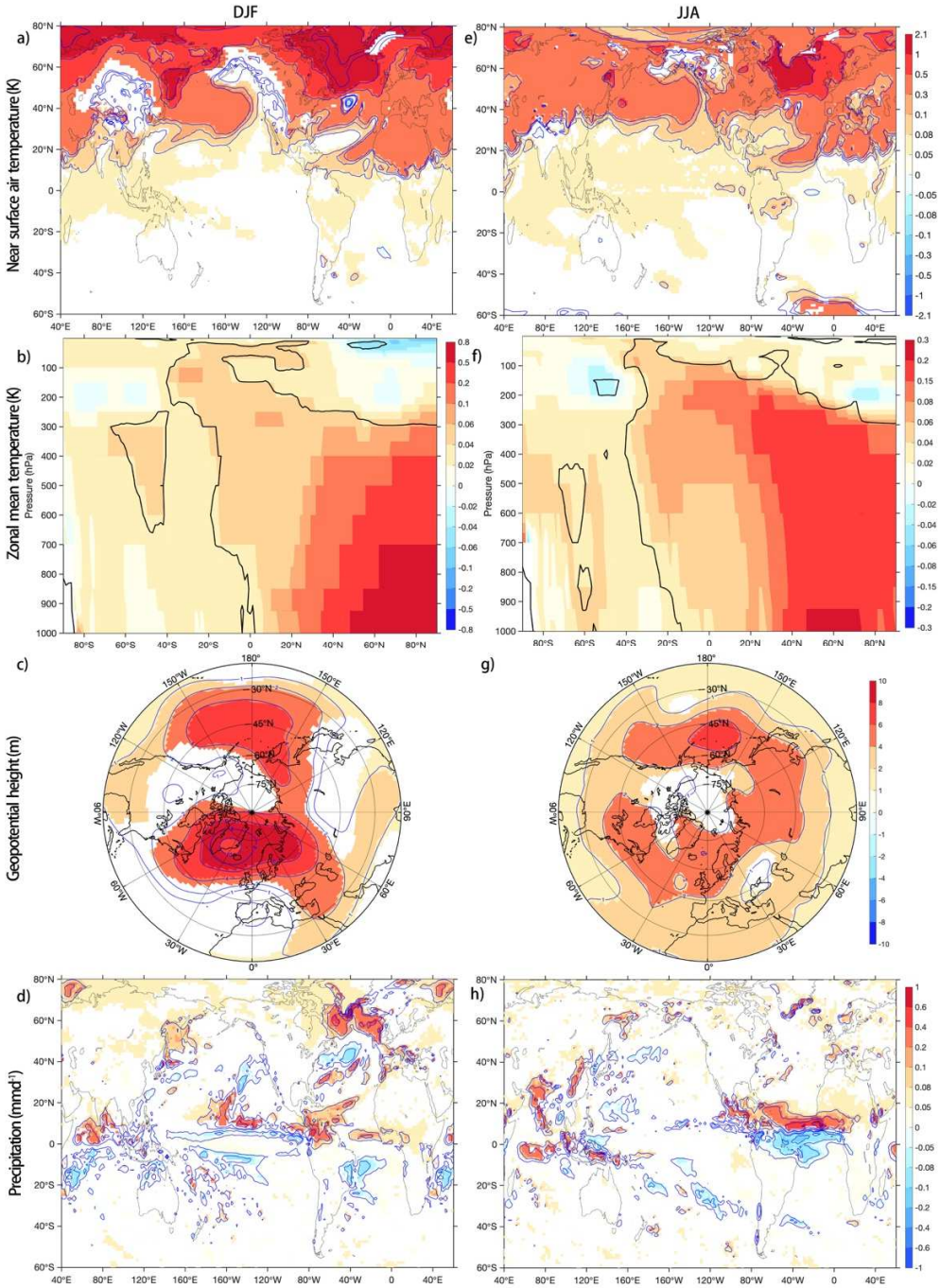

Figure 10. Regression onto AMOC LFC1 of various climate fields in winter (DJF, (a)-(d)) and summer (JJA, (e)-(h)), when the AMOC leads by 10-yr: (a) Air temperature at 2m height, in K, (b) zonal mean air temperature, in K, (c) geopotential height at 500hPa, in m. (d) Precipitation, in mm d^{-1}. In (a), (b) and (d), colors are shown if anomalies are statistically significant at 5% level, while blue contours intervals correspond to that shown in color bar. In (d), black contours indicate significance level at 5%. (e)-(h) are the same as (a)-(d), but for summer. Note the different color scale in (b) and (f).

Accepted Article

This article is protected by copyright. All rights reserved.

The atmospheric changes associated with the AMOC variations are quite similar from lag -10-yr to lag 10-yr. To better evaluate the atmosphere's response to the AMOC variations and separate it from the atmospheric forcing, we show in Fig. 10 the regressions when the AMOC leads by 10-yr, but the results presented next are hardly modified for lag 0-yr and lag -10-yr.

Associated with the strong AMOC and increased northward heat transport, the Arctic warms by ~1.5°C in winter and ~0.8°C in summer. The amplification of the warming in winter is likely linked to the anomalous heat release from the ocean to the atmosphere associated with sea ice loss (Deser et al., 2015) and to the North Atlantic warming. The Arctic atmosphere being more stable near the surface in winter, the warming is confined to the lower troposphere (Pithan & Mauritsen, 2014), while it reaches 400-hPa or 300-hPa in summer. Aside from the polar region, the entire Northern Hemisphere north of 20°N also warms by ~0.5°C, and the tropics between 20°S and 20°N show a weak warming of ~0.05°C (Fig. 10a and e). The zonal-mean tropospheric temperature shows a local warming maximum in the tropical upper troposphere (Fig.10b and f), following changes in the moist adiabat (Chiang & Bitz, 2005; Zhang et al., 2017). It is larger in summer, as the SST anomalies are warmer, and possibly because deep convection occurs more frequently in the Northern Hemisphere. These tropospheric temperature anomalies resemble the 'mini global warming' pattern found in many modeling works simulating the Arctic sea ice loss (e.g., Deser et al., 2015; Sun et al., 2018; Screen et al., 2018; Liu & Fedorov, 2019). However, in those cases, sea ice loss is imposed, and the resulting warming and freshwater release lead to an AMOC decrease. In IPSL-CM6A-LR, the intrinsic variability shows instead simultaneous AMOC increase and Arctic sea ice extent decrease.

In summer, the geopotential height at 500-hPa increases uniformly in the Northern Hemisphere, with a larger amplitude at high latitudes (Fig. 10c and g). At the same time, the SLP anomalies are negative over the Arctic and North Atlantic Ocean (not shown at lag 10, but similar to Fig. 5c at lag -10), indicating a thermal low structure resulting from the heating of the lower troposphere. The situation is similar in winter, apart from some small positive SLP anomalies over the Arctic sea-ice edges (not shown). An exception to this baroclinic structure is the SLP and geopotential height increase over the Aleutians. This could be related to the relative cooling of the Equatorial Pacific in winter, itself possibly a consequence of the warm surface anomalies in the Atlantic Ocean driving La Niña-like anomalies through a reorganization of the Walker circulation (Polo et al., 2015; Ruprich-Robert et al., 2017).

Another typical pattern associated with a warming Northern Hemisphere and an intensified AMOC is the northward shift of the ITCZ. Precipitation indeed increases north of the equator and decreases south of the equator, especially over the tropical Atlantic in summer (Fig. 10h) and over the Indo-Pacific in winter (Fig. 10d). This displacement causes more summertime rainfall in the Caribbean, African Sahel, and the Indian and Asian monsoon regions but less in Brazil (Fig. 10h). Similar responses of rainfall to a strong AMOC are found in other models (Folland et al., 2001; Sutton & Hodson, 2005; Smith et al., 2017) as well as in observations (Folland et al., 1986; Zhang & Delworth, 2006). An explanation involving the energy budget was put forward in atmospheric model simulations coupled to a mixed layer ocean (L'Heveder et al., 2015; Kang et al., 2008; Frierson et al., 2013; Tomas et al., 2016): to balance the anomalous northward cross-equatorial energy transport by a stronger AMOC, the atmosphere needs to transport energy southward. In the Tropics, this is accomplished by a cross-equatorial Hadley circulation, transporting total energy in the direction of its upper branch. The anomalous near-surface circulation is then northward, transporting more moisture into the northern hemisphere and leading to a northward shift of the ITCZ.

Accepted Article

This article is protected by copyright. All rights reserved.

Accepted Article

4 Discussion and conclusions

The variability emerging from the North Atlantic and Arctic oceans in the 2000-yr IPSL-CM6-LR pre-industrial control simulation is dominated by multi-centennial fluctuations, as previously noted in Boucher et al. (2020). We show that this multi-centennial variability is caused by delayed oceanic freshwater exchanges between the North Atlantic and the Arctic, with little influence of the atmospheric forcing. The AMOC changes are driven by density anomalies in the deep convective regions, caused by salinity anomalies. The cycle starts with the build-up of a positive salinity anomaly around Greenland, increasing the surface seawater density and the deep convection in the Labrador and Nordic Seas. This leads to an intensified AMOC, and the associated heat transport causes a surface warming in the North Atlantic. The associated warming of the lower troposphere then warms the ocean and melts the sea ice. A negative salinity anomaly thus appears at the surface in the Central Arctic. This freshwater anomaly builds up progressively, in thermal wind balance with an anomalous anticyclonic circulation that helps to maintain it inside the Arctic. Meanwhile, the advection of the positive salt anomaly by the mean inflow of Atlantic water leads to a positive salinity anomaly over the Laptev and East-Siberian seas. The freshwater anomalies in Central Arctic broaden during 4 to 5 decades until they reach the Lincoln Sea north of Greenland. Then, the salinity anomalies around Greenland change sign to become negative, associated with a faster anticyclonic circulation. Eventually, the anomalous freshwater spreads to the convection sites in the Nordic and Labrador Seas, the AMOC decreases and the oscillation shifts to the opposite phase, with positive salt anomalies propagating from Eastern Arctic to Central Arctic.

The investigation of salt tendencies reveals that the parameterized diffusion does not play a significant role, as expected from the low mixing in polar region (de Lavergne et al., 2015). Thus, we suggest that the multi-centennial timescale emerges mostly from the freshwater holding capacity in the central Arctic, and the interplay between this central freshwater pool and the circulation circling Greenland. Besides, we speculate that the salt anomalies advected by the Atlantic inflow into the Eastern Arctic are acting as a negative feedback, reversing the sign of the Arctic freshwater content anomalies. The oceanic circulation over the continental shelf in the East Siberian Sea and the Laptev Sea might bring the subsurface salty Atlantic water to reach the surface. However, the actual pathway of the salt anomaly remains to be fully understood with tools such as Lagrangian tracers. More work is also needed to quantify the advective time scales involved to fully understand this Arctic freshwater holding capacity as well as the mixing processes in the Laptev and East-Siberian Seas.

The primary driving mechanism in our study reminds of the one proposed by Jungclaus et al. (2005, J05), in which the anomalous freshwater exchanges between the Arctic and North Atlantic are also the key driving factor, but with some important differences. First, their period is shorter, about 70-80yr, and the deep convection is not in phase in the Labrador and Nordic Seas. The initial reduction in sea ice export results from anticyclonic circulation anomalies in the Greenland Sea caused by ocean warming, and the geopotential height difference between the Greenland Sea and the Arctic Ocean. But in our study, the influence of temperature does not contribute to the density anomalies in the regions of interest. We also find that current and salinity anomalies are in phase in the EGC, unlike in Jungclaus et al. (2005). Besides, in our case, the atmospheric circulation anomalies remain small and hardly statistically significant. More generally, the accumulation of freshwater in the central Arctic seems to play a larger role in our case, rather than circulation changes in the Nordic Seas .

We did not find significant salinity anomalies propagating from the Southern Ocean, which is the key mechanism proposed in Delworth and Zeng (2012). Some negative salinity anomalies in the subtropical Atlantic are found associated with the ITCZ northward shift, as in Vellinga and Wu (2004) or Jackson and Vellinga (2013), but these anomalies are much weaker than those

This article is protected by copyright. All rights reserved.

propagating from the Arctic. Therefore, we suggest that they do not have an active role in the centennial variability.

A strong AMOC phase shows significant climate impacts, with a Northern Hemisphere warming, maximum in winter. The warming is mainly baroclinic over North Atlantic and Arctic, with only a few sea-level-pressure changes, as found in a previous study focusing on the impacts of North Atlantic warming (Ruprich-Robert et al., 2017). We also found an important northward shift of the ITCZ, influencing both the West African and Indian monsoon. All these impacts are consistent with a Northern Hemisphere warming caused by Arctic sea ice reduction and AMOC intensification. Further work would be needed to distinguish the specific role for climate of the AMOC from the sea-ice loss and polar amplification feedbacks.

Although such multi-centennial variability is not as dominant as the multi-decadal variability, climate proxies indicate that a centennial to multi-centennial North Atlantic variability exists (Mann et al., 1995; Laepple & Huybers, 2013; Ayache et al., 2018). More work is still needed to further assess the realism of the variability found in IPSL-CM6A-LR with proxy data. Similar centennial variability also occurs in other climate models participating in CMIP6. CNRM-CM6 (Voldoire et al., 2019) has an even more dominant centennial variability, while EC-Earth3.3 has a comparable one (Y. Ruprich-Robert; personal communication). As EC-Earth3.3 and CNRM-CM6 share the same oceanic component as IPSL-CM6-LR, i.e., NEMOv6 with a 1° nominal resolution, but with a different embedded sea-ice module in the case of CNRM-CM6, the question about the properties within the ocean favoring the emergence of such centennial variability remains open. Our results suggest that such variability is characterized by an alternating salinity anomaly between the Central Arctic and at the coast of Greenland. A better understanding of the freshwater budget over these specific locations is needed to investigate the relevant evolution. Besides, the rapid adjustment of salinity anomalies around Greenland could be exacerbated by an over-simplistic bathymetry around Greenland, with the Nares strait being too deep (Fig. S2b). However, multi-centennial sensitivity experiments would be required to further assess the role of bathymetry.

Lastly, human activities are estimated to have caused approximately 1°C of global warming above pre-industrial levels (IPCC, 2018). The presence of such centennial variability might potentially regulate and cover up the anthropogenic-driven climate change. Therefore, ongoing efforts aim to assess the signature of centennial to multi-centennial variability in the warming climate and investigate how it impacts the historical and scenario simulation in terms of spread or uncertainty.

Acknowledgment:

We thank two anonymous reviewers for their constructive suggestions and comments. We also acknowledge the developers of SOSIE version 3.0 and CDFTOOLS package, that we used to rotate the current from the tri-polar ORCA grid to the geographic domain (SOSIE), calculate the oceanic transports through sections and approximate geographical sections with proper adjacent grid points (CDFTOOLS). GG and FC were supported by the Blue-Action project (European Union's Horizon 2020 research and innovation program, grant number: 727852), WJ by a grant from the MOPGA project and EUR-IPSL. This work used the HPC resources of TGCC under the allocations 2016-A0030107732, 2017-R0040110492 and 2018-1293R0040110492 (project gencmip6) provided by GENCI (Grand Equipement National de Calcul Intensif). This study benefited from the ESPRI (Ensemble de Services Pour la Recherche à l'IPSL) computing and data center (https://mesocentre.ipsl.fr) which is supported by CNRS, Sorbonne Université, Ecole Polytechnique and CNES and through national and international grants. The data of the simulation presented here is available on ESGF-CMIP6 (DOI: 10.22033/ESGF/CMIP6.1534).

This article is protected by copyright. All rights reserved.

Accepted Article

Accepted Article

References

Aksenov, Y., Ivanov, V. V., Nurser, A. J. G., Bacon, S., Polyakov, I. V., Coward, A. C., et al. (2011). The Arctic Circumpolar Boundary Current. *Journal of Geophysical Research: Oceans*, *116*(C9). https://doi.org/10.1029/2010JC006637

Ayache, M., Swingedouw, D., Mary, Y., Eynaud, F., & Colin, C. (2018). Multi-centennial variability of the AMOC over the Holocene: A new reconstruction based on multiple proxy-derived SST records. *Global and Planetary Change*, *170*, 172–189. https://doi.org/10.1016/j.gloplacha.2018.08.016

Boucher, O., Servonnat, J., Albright, A. L., Aumont, O., Balkanski, Y., Bastrikov, V., et al. (n.d.). Presentation and evaluation of the IPSL-CM6A-LR climate model. *Journal of Advances in Modeling Earth Systems*, *n/a*(n/a), e2019MS002010. https://doi.org/10.1029/2019MS002010

Brown, P. T., Lozier, M. S., Zhang, R., & Li, W. (2016). The necessity of cloud feedback for a basin-scale Atlantic Multidecadal Oscillation. *Geophysical Research Letters*, *43*(8), 3955–3963. https://doi.org/10.1002/2016GL068303

Cane, M. A., Clement, A. C., Murphy, L. N., & Bellomo, K. (2017). Low-Pass Filtering, Heat Flux, and Atlantic Multidecadal Variability. *Journal of Climate*, *30*(18), 7529–7553. https://doi.org/10.1175/JCLI-D-16-0810.1

Cassou, C., Kushnir, Y., Hawkins, E., Pirani, A., Kucharski, F., Kang, I.-S., & Caltabiano, N. (2018). Decadal Climate Variability and Predictability: Challenges and Opportunities. *Bulletin of the American Meteorological Society*, *99*(3), 479–490. https://doi.org/10.1175/BAMS-D-16-0286.1

Chiang, J. C. H., & Bitz, C. M. (2005). Influence of high latitude ice cover on the marine Intertropical Convergence Zone. *Climate Dynamics*, *25*(5), 477–496. https://doi.org/10.1007/s00382-005-0040-5

Clement, A., Bellomo, K., Murphy, L. N., Cane, M. A., Mauritsen, T., Rädel, G., & Stevens, B. (2015). The Atlantic Multidecadal Oscillation without a role for ocean circulation. *Science*, *350*(6258), 320–324. https://doi.org/10.1126/science.aab3980

Colfescu, I., & Schneider, E. K. (2020). Decomposition of the Atlantic Multidecadal Variability in a Historical Climate Simulation. *Journal of Climate*, *33*(10), 4229–4254. https://doi.org/10.1175/JCLI-D-18-0180.1

Cunningham, S. A., Kanzow, T., Rayner, D., Baringer, M. O., Johns, W. E., Marotzke, J., et al. (2007). Temporal Variability of the Atlantic Meridional Overturning Circulation at 26.5°N. *Science*, *317*(5840), 935–938. https://doi.org/10.1126/science.1141304

Danabasoglu, G. (2008). On Multidecadal Variability of the Atlantic Meridional Overturning Circulation in the Community Climate System Model Version 3. *Journal of Climate*, *21*(21), 5524–5544. https://doi.org/10.1175/2008JCLI2019.1

De Lavergne, C., Madec, G., Le Sommer, J., Nurser, A. G., & Naveira Garabato, A. C. (2016). The impact of a variable mixing efficiency on the abyssal overturning. *Journal of Physical* Oceanography, 46(2), 663-681.

Delworth, Thomas L., & Zeng, F. (2012). Multicentennial variability of the Atlantic meridional overturning circulation and its climatic influence in a 4000 year simulation of the GFDL CM2.1 climate model: MULTICENTENNIAL CLIMATE VARIABILITY. *Geophysical Research Letters*, *39*(13), n/a-n/a. https://doi.org/10.1029/2012GL052107

Deser, C., Tomas, R. A., & Sun, L. (2015). The Role of Ocean–Atmosphere Coupling in the Zonal-Mean Atmospheric Response to Arctic Sea Ice Loss. *Journal of Climate*, *28*(6), 2168–2186. https://doi.org/10.1175/JCLI-D-14-00325.1

This article is protected by copyright. All rights reserved.

Accepted Article

Drews, A., & Greatbatch, R. J. (2017). Evolution of the Atlantic Multidecadal Variability in a Model with an Improved North Atlantic Current. *Journal of Climate*, 30(14), 5491–5512. https://doi.org/10.1175/JCLI-D-16-0790.1

Ebisuzaki, W. (1997). A Method to Estimate the Statistical Significance of a Correlation When the Data Are Serially Correlated. *Journal of Climate*, *10*(9), 2147–2153. https://doi.org/10.1175/1520-0442(1997)010<2147:AMTETS>2.0.CO;2

Eden, C., & Willebrand, J. (2001). Mechanism of Interannual to Decadal Variability of the North Atlantic Circulation. *Journal of Climate*, *14*(10), 2266–2280. https://doi.org/10.1175/1520-0442(2001)014<2266:MOITDV>2.0.CO;2

Escudier, R., Mignot, J., & Swingedouw, D. (2013). A 20-year coupled ocean-sea ice-atmosphere variability mode in the North Atlantic in an AOGCM. *Climate Dynamics*, *40*(3), 619–636. https://doi.org/10.1007/s00382-012-1402-4

Eyring, V., Bony, S., Meehl, G. A., Senior, C. A., Stevens, B., Stouffer, R. J., & Taylor, K. E. (2016). Overview of the Coupled Model Intercomparison Project Phase 6 (CMIP6) experimental design and organization. *Geoscientific Model Development*, *9*(5), 1937–1958. https://doi.org/10.5194/gmd-9-1937-2016

Flato, G., J. Marotzke, B. Abiodun, P. Braconnot, S.C. Chou, W. Collins, P. Cox, F. Driouech, S. Emori, V. Eyring, C. Forest, P. Gleckler, E. Guilyardi, C. Jakob, V. Kattsov, C. Reason, and M. Rummukainen, 2013: Evaluation of climate models. In *Climate Change 2013: The Physical Science Basis. Contribution of Working Group I to the Fifth Assessment Report of the Intergovernmental Panel on Climate Change*. T.F. Stocker, D. Qin, G.-K. Plattner, M. Tignor, S.K. Allen, J. Doschung, A. Nauels, Y. Xia, V. Bex, and P.M. Midgley, Eds. Cambridge University Press, pp. 741-882, doi:10.1017/CBO9781107415324.020.

Folland, C. K., Palmer, T. N., & Parker, D. E. (1986). Sahel rainfall and worldwide sea temperatures, 1901–85. *Nature*, *320*(6063), 602–607. https://doi.org/10.1038/320602a0

Folland, Chris K., Colman, A. W., Rowell, D. P., & Davey, M. K. (2001). Predictability of Northeast Brazil Rainfall and Real-Time Forecast Skill, 1987–98. *Journal of Climate*, *14*(9), 1937–1958. https://doi.org/10.1175/1520-0442(2001)014<1937:PONBRA>2.0.CO;2

Frankcombe, L. M., von der Heydt, A., & Dijkstra, H. A. (2010). North Atlantic Multidecadal Climate Variability: An Investigation of Dominant Time Scales and Processes. *Journal of Climate*, *23*(13), 3626–3638. https://doi.org/10.1175/2010JCLI3471.1

Frierson, D. M. W., Hwang, Y.-T., Fučkar, N. S., Seager, R., Kang, S. M., Donohoe, A., et al. (2013). Contribution of ocean overturning circulation to tropical rainfall peak in the Northern Hemisphere. *Nature Geoscience*, *6*(11), 940–944. https://doi.org/10.1038/ngeo1987

Häkkinen, S., Rhines, P. B., & Worthen, D. L. (2011). Atmospheric Blocking and Atlantic Multidecadal Ocean Variability. *Science*, *334*(6056), 655–659. https://doi.org/10.1126/science.1205683

Hawkins, E., & Sutton, R. (2007). Variability of the Atlantic thermohaline circulation described by three-dimensional empirical orthogonal functions. *Climate Dynamics*, *29*(7–8), 745–762. https://doi.org/10.1007/s00382-007-0263-8

IPCC, 2018: Global Warming of 1.5°C. *An IPCC Special Report on the impacts of global warming of 1.5°C above pre-industrial levels and related global greenhouse gas emission pathways, in the context of strengthening the global response to the threat of climate change, sustainable development, and efforts to eradicate poverty* [Masson-Delmotte, V., P. Zhai, H.-O. Pörtner, D. Roberts, J. Skea, P.R. Shukla, A. Pirani, W. Moufouma-Okia, C. Péan, R. Pidcock, S. Connors, J.B.R. Matthews, Y. Chen, X. Zhou, M.I. Gomis, E. Lonnoy, T. Maycock, M. Tignor, and T. Waterfield (eds.)]. In Press.

This article is protected by copyright. All rights reserved.

Accepted Article

Jackson, L., & Vellinga, M. (2013). Multidecadal to Centennial Variability of the AMOC: HadCM3 and a Perturbed Physics Ensemble. *Journal of Climate*, *26*(7), 2390–2407. https://doi.org/10.1175/JCLI-D-11-00601.1

Jackson, L. C., Kahana, R., Graham, T., Ringer, M. A., Woollings, T., Mecking, J. V., & Wood, R. A. (2015). Global and European climate impacts of a slowdown of the AMOC in a high resolution GCM. *Climate Dynamics*, *45*(11), 3299–3316. https://doi.org/10.1007/s00382-015-2540-2

Jahn, A., & Holland, M. M. (2013). Implications of Arctic sea ice changes for North Atlantic deep convection and the meridional overturning circulation in CCSM4-CMIP5 simulations. *Geophysical Research Letters*, *40*(6), 1206–1211. https://doi.org/10.1002/grl.50183

Jungclaus, J. H., Haak, H., Latif, M., & Mikolajewicz, U. (2005). Arctic–North Atlantic Interactions and Multidecadal Variability of the Meridional Overturning Circulation. *Journal of Climate*, *18*(19), 4013–4031. https://doi.org/10.1175/JCLI3462.1

Kang, S. M., Held, I. M., Frierson, D. M. W., & Zhao, M. (2008). The Response of the ITCZ to Extratropical Thermal Forcing: Idealized Slab-Ocean Experiments with a GCM. *Journal of Climate*, *21*(14), 3521–3532. https://doi.org/10.1175/2007JCLI2146.1

Kerr, R. A. (2000). A North Atlantic Climate Pacemaker for the Centuries. *Science*, *288*(5473), 1984–1985. https://doi.org/10.1126/science.288.5473.1984

Knight, J. R., Allan, R. J., Folland, C. K., Vellinga, M., & Mann, M. E. (2005). A signature of persistent natural thermohaline circulation cycles in observed climate. *Geophysical Research Letters*, *32*(20). https://doi.org/10.1029/2005GL024233

Laepple, T., & Huybers, P. (2013). Reconciling discrepancies between Uk37 and Mg/Ca reconstructions of Holocene marine temperature variability. *Earth and Planetary Science Letters*, *375*, 418–429. https://doi.org/10.1016/j.epsl.2013.06.006

L'Hévéder, B., Codron, F., & Ghil, M. (2015). Impact of Anomalous Northward Oceanic Heat Transport on Global Climate in a Slab Ocean Setting. *Journal of Climate*, *28*(7), 2650–2664. https://doi.org/10.1175/JCLI-D-14-00377.1

Liu, W., & Fedorov, A. V. (2019). Global Impacts of Arctic Sea Ice Loss Mediated by the Atlantic Meridional Overturning Circulation. *Geophysical Research Letters*, *46*(2), 944–952. https://doi.org/10.1029/2018GL080602

Lique, C., Treguier, A. M., Scheinert, M., & Penduff, T. (2009). A model-based study of ice and freshwater transport variability along both sides of Greenland. *Climate Dynamics*, *33*(5), 685–705. https://doi.org/10.1007/s00382-008-0510-7

Locarnini, R. A., A. V. Mishonov, O. K. Baranova, T. P. Boyer, M. M. Zweng, H. E. Garcia, J. R. Reagan, D. Seidov, K. Weathers, C. R. Paver, and I. Smolyar, 2018. *World Ocean Atlas 2018, Volume 1: Temperature.* A. Mishonov Technical Ed.; NOAA Atlas NESDIS 81, 52 pp.

Mahajan, S., Zhang, R., & Delworth, T. L. (2011). Impact of the Atlantic Meridional Overturning Circulation (AMOC) on Arctic Surface Air Temperature and Sea Ice Variability. *Journal of Climate*, *24*(24), 6573–6581. https://doi.org/10.1175/2011JCLI4002.1

Mann, M. E., Park, J., & Bradley, R. S. (1995). Global interdecadal and century-scale climate oscillations during the past five centuries. *Nature*, *378*(6554), 266–270. https://doi.org/10.1038/378266a0

Muir, L. C., & Fedorov, A. V. (2015). How the AMOC affects ocean temperatures on decadal to centennial timescales: the North Atlantic versus an interhemispheric seesaw. *Climate Dynamics*, *45*(1), 151–160. https://doi.org/10.1007/s00382-014-2443-7

This article is protected by copyright. All rights reserved.

Murphy, L. N., Bellomo, K., Cane, M., & Clement, A. (2017). The role of historical forcings in simulating the observed Atlantic multidecadal oscillation. *Geophysical Research Letters*, 44(5), 2472-2480.

Nigam, S., Guan, B., & Ruiz□Barradas, A. (2011). Key role of the Atlantic Multidecadal Oscillation in 20th century drought and wet periods over the Great Plains. *Geophysical Research Letters*, *38*(16). https://doi.org/10.1029/2011GL048650

Notz, D., Jahn, A., Holland, M., Hunke, E., Massonnet, F., Stroeve, J., et al. (2016). The CMIP6 Sea-Ice Model Intercomparison Project (SIMIP): understanding sea ice through climate-model simulations. *Geoscientific Model Development*, *9*(9), 3427–3446. https://doi.org/10.5194/gmd-9-3427-2016

Nyberg, J., Malmgren, B. A., Kuijpers, A., & Winter, A. (2002). A centennial-scale variability of tropical North Atlantic surface hydrography during the late Holocene. *Palaeogeography, Palaeoclimatology, Palaeoecology*, *183*(1), 25–41. https://doi.org/10.1016/S0031-0182(01)00446-1

Ortega, P., Mignot, J., Swingedouw, D., Sévellec, F., & Guilyardi, E. (2015). Reconciling two alternative mechanisms behind bi-decadal variability in the North Atlantic. *Progress in Oceanography*, *137*, 237–249. https://doi.org/10.1016/j.pocean.2015.06.009

Pardaens, A., Vellinga, M., Wu, P., & Ingleby, B. (2008). Large-Scale Atlantic Salinity Changes over the Last Half-Century: A Model–Observation Comparison. *Journal of Climate*, *21*(8), 1698–1720. https://doi.org/10.1175/2007JCLI1988.1

Park, W., & Latif, M. (2008). Multidecadal and multicentennial variability of the meridional overturning circulation. *Geophysical Research Letters*, *35*(22). https://doi.org/10.1029/2008GL035779

Petty, A. A., Hutchings, J. K., Richter□Menge, J. A., & Tschudi, M. A. (2016). Sea ice circulation around the Beaufort Gyre: The changing role of wind forcing and the sea ice state. *Journal of Geophysical Research: Oceans*, *121*(5), 3278–3296. https://doi.org/10.1002/2015JC010903

Pithan, F., & Mauritsen, T. (2014). Arctic amplification dominated by temperature feedbacks in contemporary climate models. *Nature Geoscience*, *7*(3), 181–184. https://doi.org/10.1038/ngeo2071

Pnyushkov, A. V., Polyakov, I. V., Ivanov, V. V., Aksenov, Y., Coward, A. C., Janout, M., & Rabe, B. (2015). Structure and variability of the boundary current in the Eurasian Basin of the Arctic Ocean. *Deep Sea Research Part I: Oceanographic Research Papers*, *101*, 80–97. https://doi.org/10.1016/j.dsr.2015.03.001

Polo, I., Martin-Rey, M., Rodriguez-Fonseca, B., Kucharski, F., & Mechoso, C. R. (2015). Processes in the Pacific La Niña onset triggered by the Atlantic Niño. *Climate Dynamics*, *44*(1), 115–131. https://doi.org/10.1007/s00382-014-2354-7

Proshutinsky, A., Krishfield, R., Timmermans, M.-L., Toole, J., Carmack, E., McLaughlin, F., et al. (2009). Beaufort Gyre freshwater reservoir: State and variability from observations. *Journal of Geophysical Research: Oceans*, *114*(C1). https://doi.org/10.1029/2008JC005104

Qin, M., Dai, A., & Hua, W. (2020). Quantifying contributions of internal variability and external forcing to Atlantic multidecadal variability since 1870. *Geophysical Research Letters*, 47(22), e2020GL089504.

Roberts, C. D., Garry, F. K., & Jackson, L. C. (2013). A Multimodel Study of Sea Surface Temperature and Subsurface Density Fingerprints of the Atlantic Meridional Overturning Circulation. *Journal of Climate*, *26*(22), 9155–9174. https://doi.org/10.1175/JCLI-D-12-00762.1

Accepted Article

This article is protected by copyright. All rights reserved.

Ruprich-Robert, Y., Msadek, R., Castruccio, F., Yeager, S., Delworth, T., & Danabasoglu, G. (2017). Assessing the Climate Impacts of the Observed Atlantic Multidecadal Variability Using the GFDL CM2.1 and NCAR CESM1 Global Coupled Models. *Journal of Climate*, *30*(8), 2785–2810. https://doi.org/10.1175/JCLI-D-16-0127.1

Screen, J. A., Deser, C., Smith, D. M., Zhang, X., Blackport, R., Kushner, P. J., et al. (2018). Consistency and discrepancy in the atmospheric response to Arctic sea-ice loss across climate models. *Nature Geoscience*, *11*(3), 155–163. https://doi.org/10.1038/s41561-018-0059-y

Sicre, M.-A., Yiou, P., Eiríksson, J., Ezat, U., Guimbaut, E., Dahhaoui, I., et al. (2008). A 4500-year reconstruction of sea surface temperature variability at decadal time-scales off North Iceland. *Quaternary Science Reviews*, *27*(21), 2041–2047. https://doi.org/10.1016/j.quascirev.2008.08.009

Smith, D. M., Dunstone, N. J., Scaife, A. A., Fiedler, E. K., Copsey, D., & Hardiman, S. C. (2017). Atmospheric Response to Arctic and Antarctic Sea Ice: The Importance of Ocean–Atmosphere Coupling and the Background State. *Journal of Climate*, *30*(12), 4547–4565. https://doi.org/10.2307/26388076

Stocker, T. F. (1998). The Seesaw Effect. *Science*, *282*(5386), 61–62. https://doi.org/10.1126/science.282.5386.61

Sun, L., Alexander, M., & Deser, C. (2018). Evolution of the Global Coupled Climate Response to Arctic Sea Ice Loss during 1990–2090 and Its Contribution to Climate Change. *Journal of Climate*, *31*(19), 7823–7843. https://doi.org/10.1175/JCLI-D-18-0134.1

Sutton, R. T., & Hodson, D. L. R. (2005). Atlantic Ocean Forcing of North American and European Summer Climate. *Science*, *309*(5731), 115–118. https://doi.org/10.1126/science.1109496

Tomas, R. A., Deser, C., & Sun, L. (2016). The Role of Ocean Heat Transport in the Global Climate Response to Projected Arctic Sea Ice Loss. *Journal of Climate*, *29*(19), 6841–6859. https://doi.org/10.1175/JCLI-D-15-0651.1

Vellinga, M., & Wu, P. (2004). Low-Latitude Freshwater Influence on Centennial Variability of the Atlantic Thermohaline Circulation. *Journal of Climate*, *17*(23), 4498–4511. https://doi.org/10.1175/3219.1

Voldoire, A., Saint□Martin, D., Sénési, S., Decharme, B., Alias, A., Chevallier, M., et al. (2019). Evaluation of CMIP6 DECK Experiments With CNRM-CM6-1. *Journal of Advances in Modeling Earth Systems*, *11*(7), 2177–2213. https://doi.org/10.1029/2019MS001683

Wang, C., Zhang, L., Lee, S.-K., Wu, L., & Mechoso, C. R. (2014). A global perspective on CMIP5 climate model biases. *Nature Climate Change*, *4*(3), 201–205. https://doi.org/10.1038/nclimate2118

Wills, R. C., Schneider, T., Wallace, J. M., Battisti, D. S., & Hartmann, D. L. (2018). Disentangling Global Warming, Multidecadal Variability, and El Niño in Pacific Temperatures. *Geophysical Research Letters*, *45*(5), 2487–2496. https://doi.org/10.1002/2017GL076327

Xu, X., Chassignet, E. P., & Wang, F. (2019). On the variability of the Atlantic meridional overturning circulation transports in coupled CMIP5 simulations. *Climate Dynamics*, *52*(11), 6511–6531. https://doi.org/10.1007/s00382-018-4529-0

Zhang, L., Delworth, T. L., & Zeng, F. (2017). The impact of multidecadal Atlantic meridional overturning circulation variations on the Southern Ocean. *Climate Dynamics*, *48*(5), 2065–2085. https://doi.org/10.1007/s00382-016-3190-8

Accepted Article

This article is protected by copyright. All rights reserved.

Zhang, R., & Delworth, T. L. (2006). Impact of Atlantic multidecadal oscillations on India/Sahel rainfall and Atlantic hurricanes. *Geophysical Research Letters*, *33*(17). https://doi.org/10.1029/2006GL026267

Zhang, R., Sutton, R., Danabasoglu, G., Kwon, Y., Marsh, R., Yeager, S. G., et al. (2019). A Review of the Role of the Atlantic Meridional Overturning Circulation in Atlantic Multidecadal Variability and Associated Climate Impacts. *Reviews of Geophysics*, *57*(2), 316–375. https://doi.org/10.1029/2019RG000644

Zweng, M. M., J. R. Reagan, D. Seidov, T. P. Boyer, R. A. Locarnini, H. E. Garcia, A. V. Mishonov, O. K. Baranova, K. Weathers, C. R. Paver, and I. Smolyar, 2018. *World Ocean Atlas 2018, Volume 2: Salinity.* A. Mishonov Technical Ed.; NOAA Atlas NESDIS 82, 50 pp.

Accepted Article

This article is protected by copyright. All rights reserved.